MODELING AND CONTROL OF A HYDROCARBON SELECTIVE CATALYTIC REDUCTION SYSTEM FOR DIESEL EXHAUST

A Thesis

Presented to

The Faculty of the Department of Mechanical

Engineering

University of Houston

In Partial Fulfillment

of the Requirements for the Degree

Master of Science

in Mechanical Engineering

by

Oliver Rivera

August 2012

MODELING AND CONTROL OF A HYDROCARBON SELECTIVE CATALYTIC REDUCTION SYSTEM FOR DIESEL EXHAUST

Oliver Rivera

Approved:

Chair of the Committee
Matthew A. Franchek, Professor,
Mechanical Engineering

Co-Chair of the Committee
Karolos M. Grigoriadis, Professor,
Mechanical Engineering

Michael P. Harold, Professor,
Chemical Engineering

Suresh K. Khator, Associate Dean,
Cullen College of Engineering

Pradeep Sharma, Professor and Chair
Mechanical Engineering

MODELING AND CONTROL OF A HYDROCARBON SELECTIVE CATALYTIC REDUCTION SYSTEM FOR DIESEL EXHAUST

An Abstract

of a

Thesis

Presented to

The Faculty of the Department of Mechanical

Engineering

University of Houston

In Partial Fulfillment

of the Requirements for the Degree

Master of Science

in Mechanical Engineering

by

Oliver Rivera

August 2012

ABSTRACT

Diesel vehicles are continually being regulated each year by tighter restrictions on exhaust emissions. Nitrogen Oxides (NO_x) form one of the more difficult emissions to control. Urea based selective catalytic reduction (SCR) of NO_x emissions is an evolving technology that has seen widespread implementation on over the road vehicles. However, this technology requires an on-board reductant to function properly. Hydrocarbon based SCR (HC-SCR) technology eliminates the need for an additional on-board liquid by using diesel fuel as the reductant. A review of aftertreatment systems including HC-SCR is provided in this work. This review is followed by an experimental investigation of an HC-SCR aftertreatment system fitted to a marine diesel engine. A model of the HC-SCR outlet NO_x concentration is developed and validated for several operating conditions. A sensitivity analysis of the model parameters is performed, demonstrating the most influential model parameters. A controller is successfully implemented in simulation and in the laboratory environment.

TABLE OF CONTENTS

Abstract iv
Table of Contents vi
List of Figures viii
List of Tables x
Chapter I: review of diesel emission reduction systems 1
The Need for Diesel Exhaust Aftertreatment 1
Introduction 1
Nitrogen Oxide Emissions 2
Hydrocarbon Emissions 4
Particulate matter 5
Diesel Particulate Filters 7
Selective Catalytic Reduction of NO_x 9
Ammonia Injection 9
Urea Injection 10
Hydrocarbon Injection 12
Previous HC-SCR Modeling Work 14
Chapter II: Experimental Method 16
Description of Test Equipment 16
Experimental Method 21
Chapter III: Analysis 24
Basis for Modeling Approach 24
Development of the HC-SCR Model 25
Description of HC-SCR Model 30
Calibration of Model 35
Chapter IV: Validation of Model 38
Validation Over Different Data Sets 38
Sensitivity analysis 42

Health Diagnostics 43
Chapter V: Development of Control Methodology 45
Chapter VI: Conclusions and Future Work 48
Conclusions 48
Future Work 48
Bibliography 50
Appendix 52
Model Parameters and Graphs 52
Sensitivity Analysis Graphs 58

LIST OF FIGURES

Figure 1: NO_x vs. engine Torque over different tests. Measurements taken post-DPF.....3
Figure 2: Types of particulate matter.....6
Figure 3: Geometry of filter material used in DPF.....7
Figure 4: Diesel aftertreatment system including DPF and SCR, with injector and flow bypass.....17
Figure 5: Locations of thermocouples on SCR and individual brick geometry.....18
Figure 6: Histogram showing variation in engine torque.....22
Figure 7: Histogram showing variation in SCR flow.....23
Figure 8: Internal temperatures during one test session.....26
Figure 9: NO_x reduction vs. Temperature at space velocity $3108h^{-1}$, average inlet NO_x 1700ppm.....27
Figure 10: Comparison of NO_x and Injector signals over time.....28
Figure 11: Outlet NO_x vs Time showing transport delay at space velocity of $3108h^{-1}$ during light-off activity.....29
Figure 12: Simulink representation of model.....30
Figure 13: Weighting function subsystem.....31
Figure 14: Output vs. input for non-linear temperature function.....33
Figure 15: Estimated and measured NO_x outlet concentration calibrated using 12/6/2011 data, applied over 12/5/2011 data.....39
Figure 16: Estimated and measured outlet NO_x concentration calibrated using 12/21/2011 second data set, applied over 12/21/11 first data set.....40
Figure 17: A closer look at a transition within estimate of 12/21/2011 first data set, calibrated using 12/21/2011 second data set.....41
Figure 18: Estimated and measured outlet NO_x concentration calibrated using 12/21/2011 second data set, applied over 12/22/11 third data set.....42
Figure 19: Estimated and measured outlet NO_x concentration during a reductant supply failure.....44
Figure 20: Simulink block diagram showing closed loop simulation of SCR.....45

Figure 21: Simulated system under closed-loop control with 1300ppm NO_x set point 46
Figure 22: LabView screen capture during closed loop operation 47
Figure 23: Estimated and measured outlet NO_x concentration, 12/5/2011, second set 54
Figure 24: Estimated and measured outlet NO_x concentration, 12/5/2011, third set 54
Figure 25: Estimated and measured outlet NO_x concentration, 12/6/2011, second set 55
Figure 26: Estimated and measured outlet NO_x concentration, 12/19/2011, second set 55
Figure 27: Estimated and measured outlet NO_x concentration, 12/21/2011, first set 56
Figure 28: Estimated and measured outlet NO_x concentration, 12/21/2011, second set 56
Figure 29: Estimated and measured outlet NO_x concentration, 12/22/2011, third set 57
Figure 30: Estimated and measured outlet NO_x concentration, 1/10/2012, second set 57
Figure 31: Sensitivity of AAE to changes in parameter T 58
Figure 32: Sensitivity of AAE to changes in parameter a 59
Figure 33: Sensitivity of AAE to changes in parameter b 59
Figure 34: Sensitivity of AAE to changes in parameter c 60
Figure 35: Sensitivity of AAE to changes in parameter ctemp 60
Figure 36: Sensitivity of AAE to changes in parameter d (time delay) 61
Figure 37: Sensitivity of AAE to changes in parameter offset 61
Figure 38: Sensitivity of AAE to changes in parameter otemp 62
Figure 39: Sensitivity of AAE to changes in parameter y 62

LIST OF TABLES

Table 1: Cummins N14-M Specifications....16
Table 2: Thermocouple depth in catalyst....19
Table 3: Description of recorded variables....21
Table 4: Estimated delay time based on flow rate....35
Table 5: Calibrated model parameters....53

CHAPTER I: REVIEW OF DIESEL EMISSION REDUCTION SYSTEMS

The Need for Diesel Exhaust Aftertreatment

INTRODUCTION

In the past few years, clean diesel engines have started to make their way into production over the road vehicles. This has been made possible by large advancements in the handling of the diesel exhaust, innovative combustion chamber design and injector placement, and precise injector control [1]. The black cloud of soot that set apart any diesel vehicle from its gasoline counterpart is now gone, as are most of the emissions that went along with it. However, stricter exhaust regulations require ever improving technologies to be employed on the exhaust of the diesel engine as well as inside the combustion chamber. A few of these regulations, and the emissions that drive them, will be discussed in the following paragraphs.

The diesel, or compression ignition (CI), engine operates by directly injecting diesel fuel into a combustion chamber filled with high temperature, high pressure air. The temperature and pressure of the air is so high that once diesel fuel has been introduced into this environment, it begins to burn. The resultant energy of combustion is harnessed at constant pressure during the power stroke by a piston. Unlike spark ignition (SI) engines, the CI engine uses a non-homogeneous mixture of fuel and excess air. Thus the combustion reaction generates various emissions based on the development of the combustion at the onset of ignition and during the power stroke.

The United States Environmental Protection Agency (EPA) sets the regulations for vehicle tailpipe emissions. As it relates to diesels, the relevant emission constraints are placed on NO_x and particulate matter (PM). The current regulations fall under the category of Tier 2 exhaust emissions standards subdivided into 11 "bins" with different levels of allowable emissions. Starting in 2004 the Tier 2 standard required 75% of manufacturers' fleet vehicles to meet the 0.3g/mi average NO_x standard and 25% of fleet vehicles to meet the 0.07g/mi average NO_x standard. By 2007 this standard was phased in such a way that the entire vehicle fleet would meet an average of 0.07g/mi NO_x. These limits are placed at a full useful life of

150,000 miles. As mentioned earlier there are 11 bins, with Bin 1 being the most restricted emission standard and Bin 11 being the most relaxed standard. Bin 5 is the average, and has the requirement of 0.07g/mi NO_x and 0.01g/mi PM [2]. To meet the Bin 9 (during phase-in) requirements of 0.3g/mi NO_x and 0.06 g/mi PM, light duty diesel manufacturers had to optimize their injection strategies, combustion processes, and air handling of the engine. Refineries also had to provide cleaner fuels. To meet the Bin 8 requirements of 0.2g/mi NO_x and 0.02g/mi PM, manufacturers began to employ the diesel particulate filter (DPF). Finally, to meet current Bin 5 standards, manufacturers started to employ the use of NO_x reduction aftertreatment technology [3]. With Europe facing similarly stringent emissions requirements, and future emissions requirements becoming lower, diesel exhaust aftertreatment is clearly a necessity for the worldwide market.

NITROGEN OXIDE EMISSIONS

Nitrogen Oxide (NO_x) emissions in diesel engines are composed of Nitric Oxide (NO) and Nitrogen Dioxide (NO_2), with NO responsible for 70% to 90% of the NO_x emissions [4]. NO is formed when nitrogen is exposed to oxygen under high temperature and pressure. NO_2 is formed when NO is exposed to oxygen at temperatures higher than 1370 degrees Celsius [1]. In-cylinder sampling experiments show that NO concentration in the combustion chamber is highest when combustion temperature is peaking [5]. Unlike SI engines, CI engines are not able to decompose the NO formed during combustion because of the rapid decrease in pressure and temperature after combustion. This results in a "freezing" phenomenon, during which most of the NO_x formed during combustion remains at high concentration and is carried out through the exhaust.

As with other emissions, the level of NO_x concentration is known to rise with engine load. This phenomenon is illustrated in Figure 1, compiled from data recorded during the present work. A nearly linear relationship between engine-out NO_x concentration and engine load (torque) can be seen. Note that in Figure 1, any deviation from the linear behavior is caused by transients.

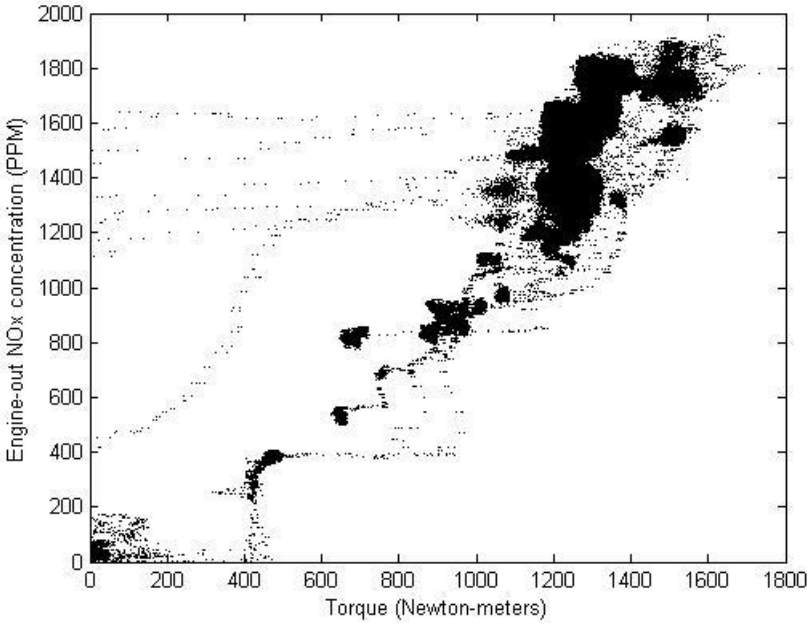

Figure 1: NO_x vs. engine Torque over different tests. Measurements taken post-DPF.

NO_x reduction has been achieved on the engine side (pre-aftertreatment) by various methods including altering injection timing, changing combustion chamber swirl characteristics and employing exhaust gas recirculation (EGR). In CI engines, the rotation of crank degrees between the start of injection to the start of ignition is known as the delay period (θ1). Increasing injection advance lengthens the delay period, since the fuel is being injected into a lower pressure and lower temperature environment [4]. Retarding the timing decreases the delay period, leaving less time for the fuel to vaporize before the start of ignition. This helps to reduce NO formation, however, using a retarded injection event requires more fuel [4]. It is also interesting to note that engines with limited speed ranges can operate with a constant delay period, while engines with larger speed ranges (such as modern passenger vehicle CI engines) require an injection advance curve to tailor the delay period with respect to engine speed to maintain high cylinder combustion pressures [1]. Thus, on modern passenger vehicle CI engines with electronic injector control, it is important to balance injection timing for both NO_x emissions and performance.

Combustion chamber swirl depends on many factors. These include injector type, injector placement, and combustion chamber (both piston and cylinder head) shape, among

others. Swirl helps to break up fuel particles and atomize the dense fuel coming into the combustion chamber. This improves combustion efficiency, however, it also causes higher combustion temperatures, which leads to generally increased NO formation [4].

EGR systems work by taking a portion of the exhaust gasses from the exhaust manifold and recirculating those inert gases back into the intake manifold. There are many different takes on the implementation of EGR. In turbocharged engines there is the option to take high pressure exhaust gasses or low pressure exhaust gasses. Whichever way the EGR system is routed, the effect on combustion is still the same: the inert gas will displace oxygen, lowering the combustion temperature and NO_x emissions. The mechanism by which this happens can be thought of in two ways. The first mechanism is thermal. The non-combustible gas introduced into the combustion chamber helps to absorb the heat of combustion, effectively acting as a heat sink. The second mechanism is chemical, that is, lowering combustion temperature by displacing oxygen [4]. One of the trade-offs of EGR is the increased particulate matter emissions. Cooling systems on the EGR help to remove heat from the incoming recirculated gasses, making the reduction of NO_x by lower combustion temperatures more effective.[1] Another benefit of cooling the EGR charge is making the recirculated gasses dense, which helps prevent displaced oxygen in the combustion chamber while still providing control of NO_x emissions.

HYDROCARBON EMISSIONS

In CI engines, hydrocarbon emissions (as most other emissions) occur because of the heterogeneous nature of the fuel and air mixture. Heywood discusses two primary methods for HC emissions to form. The first is through overly rich local mixtures, and the second is through overly lean local mixtures. HC emissions are affected by a variety of factors, most having to do with the way the fuel is injected.

One of the causes of a rich local mixture is unintended fuel drip after the injection event. The fuel dripping out of the injector is not being atomized as it enters the combustion chamber so it may not have time to completely combust, allowing HC emissions to continue on to the exhaust. This is a problem that primarily affects direct injection engines, as the

[1] For more detailed information about EGR systems see [4], [28].

injector nozzle sits in the combustion chamber. In the development of the high performance variant of the Audi 3.0l V6 bi-turbo TDI, a switch to a lower injector nozzle sac volume resulted in an approximate 36% decrease in HC emissions formation [6]. Indirect injection engines (pre-chamber engines) are not as sensitive to post-injection fuel dripping as it relates to HC emissions [5]. Another mechanism through which rich HC emissions occur is through over fueling. This can happen if the engine's fueling calibration is not correct, and more fuel is introduced into the combustion chamber than air required for stoichiometric combustion. It is interesting to note that HC emissions generally decrease as load is increased, up until reaching the equivalence ratio of 0.9, at which point HC emissions rise heavily [5]. During cold start, several of the components inside the combustion chamber have not reached a sufficient temperature to vaporize all the fuel entering the engine. The result is a misfire which allows unburned fuel to continue into the exhaust and is evidenced by white smoke at the tailpipe [4].

An overly lean air-fuel mixture in the combustion chamber is unlikely to ignite or support a flame, which leads to unburned fuel and HC formation. The lean flame out region (LFOR) refers to the outer boundary of the fuel spray over which the local air-fuel ratio is too lean to support stable combustion [4]. Advancing the injection timing, effectively increasing θ_1, generally causes HC emission levels to rise, due to the increase in LFOR area [4]. Increasing the injection pressure helps to break up and atomize the fuel as it is being injected into the combustion chamber. This also increases the LFOR area, thus increasing HC emissions.

PARTICULATE MATTER

Particulate Matter (PM) is a primarily solid emission of the diesel engine that constitutes various chemical compositions. Particulate matter is what has given the diesel engine its "dirty" image for so many years. Particulate matter is defined as exhaust particles that can be captured on a filtration medium at a temperature of 52 degrees Celsius or less. To the casual observer, this can appear as smoke emitting from the tailpipe of a diesel powered vehicle or generator, or can be detected by the odor given off by certain particulates. Particulate matter originates in the combustion chamber typically as nuclei-mode particles,

and travels through the exhaust system where the nuclei-mode particles can agglomerate with other substances into larger sized particles as they cool. These can be harmful to humans when the particles are small enough to pass through the nose and may become absorbed or remain in the lungs [1]. An outline of the composition of particulate matter in diesel exhaust is shown in Figure 2 [4].

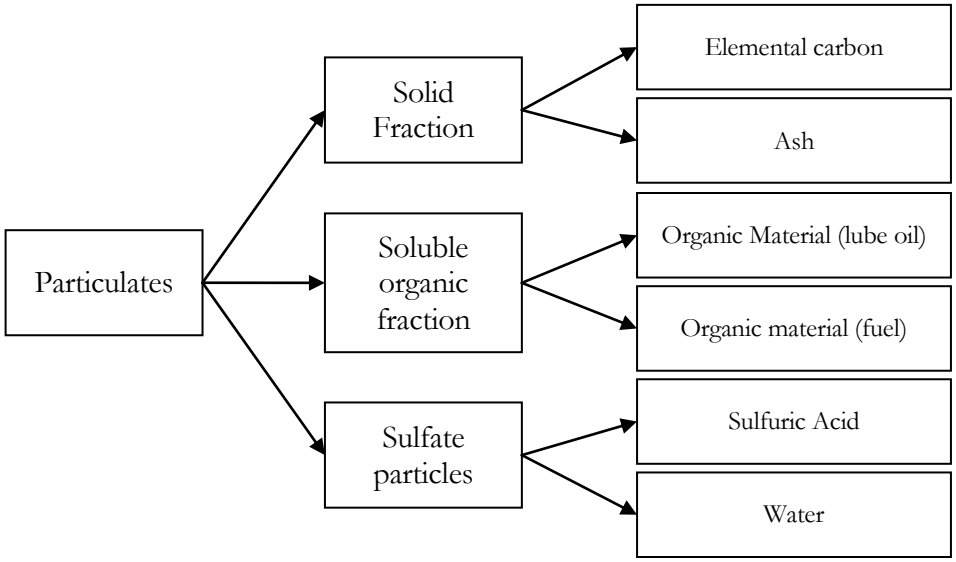

Figure 2: Types of particulate matter.

As shown in Figure 2, the solid fraction of particulate matter is composed primarily of elemental carbon and ash. Carbonaceous particles are formed in the combustion chamber and are caused by the heterogeneous nature of diesel combustion. These particulates start off as nuclei-mode and agglomerate as they make their way through the exhaust system, forming larger and even chain-like structures. Another constituent of the solid fraction of particulate matter is ash. This type of particulate matter originates from the additives in the diesel lubricating oil, engine wear particles carried into the combustion chamber, or iron oxide particles corroding from the exhaust manifold and other exhaust components. Ash is important to diesel exhaust aftertreatment design because it can be corrosive to particulate filter elements [4].

The soluble organic fraction (SOF) of diesel particulate matter is called soluble because solvents can be used to isolate the organic fraction of the particulates when analyzing

the particulate matter composition. The SOF is typically composed of lube oil based hydro-carbons, however, the percentage of lube oil based SOF can vary widely between different engines. The SOF also varies at different engine operating conditions. It was found that a cold start condition can produce 25% higher SOF levels than a hot start condition, and that SOF is highest with an engine operating at low load conditions and low exhaust temperatures [4]. High levels of SOF cannot only be attributed to a worn engine, where oil control is not optimum, but also to a poor combustion chamber design, where unburned fuel can lead to the formation of SOF particulates.

Sulfates appear in dilution tunnel experiments and are formed from the sulfuric acid and water composition of the exhaust. Sulfates are found primarily in liquid form and occur when the correct ratio of H_2O and H_2SO_4 are present. Sulfates that show up on filter material along with carbon particles can be found in the form of nuclei-mode particles [4].

Diesel Particulate Filters

The DPF is an aftertreatment device used in diesel exhaust systems to reduce the level of harmful particulate matter from the out-going exhaust. The filtration material used in a DPF is typically silicon carbide or cordierite, although metals have been used as well [7]. The filter material is arranged in such a fashion to force all the exhaust to pass through the material, as in Figure 3.

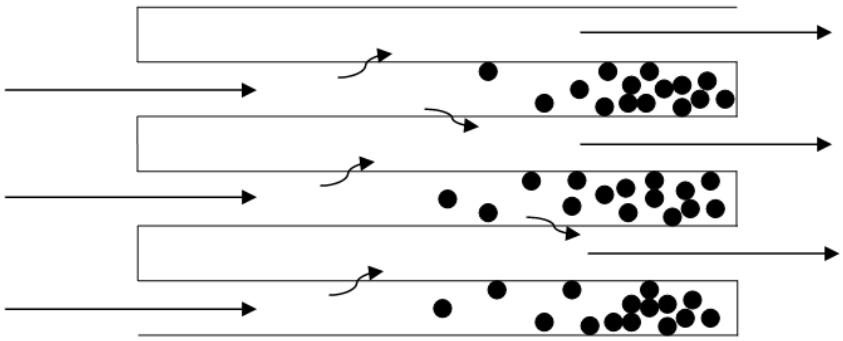

Figure 3: Geometry of filter material used in DPF.

In the above image, exhaust flows from the engine into the filtration material. The pressure of the exhaust forces the gasses to pass through the material while the harmful

particulates remain trapped in the channels of the filter. This method is proven to be capable of retaining 95% of particulate matter from the exhaust, however, to prevent build up of the particulates, regeneration is required [7]. During regeneration the particulate matter is oxidized to carbon dioxide. Most catalysts must be brought up to around 550 to 650 degrees Celsius to achieve regeneration [4]. Since most road-going diesel engines have exhaust temperatures below this range, innovative strategies are required to keep the DPF from building up with particulates and preventing adequate exhaust flow.

Typical methods for increasing exhaust temperature and therefore triggering regeneration in the DPF include using non-cooled EGR, post-injection or retarded injection timing, exhaust or intake throttle valves, bypassing the intercooler (higher inlet temperatures), and decreasing boost pressures [4]. Catalysts may be used to reduce the temperature required for regeneration. These may be used in the form of filter material coatings, or fuel additives. Coatings on the DPF can lower regeneration temperatures to roughly 325 to 420 degrees Celsius. Although fuel additives are more effective than coatings (regeneration temperatures of 300-400 degrees Celsius are typical), ash residue may be left behind in the DPF, which must be cleaned manually. Typical maintenance intervals for ash removal are in the range of 120,000 km [7].

In production applications there is a growing trend towards combining the DPF with other aftertreatment systems to provide a complete emissions reduction package. When developing their aftertreatment system for the 2.0l TDI, Volkswagen combined a diesel oxidation catalyst (DOC) with the DPF in the same canister. The exothermic oxidation of hydrocarbons by the DOC helps with generating higher exhaust temperatures near the DPF to improve regeneration. Furthermore, the DPF catalyst coating was selected carefully to provide an optimum ratio of NO_2 to NO_x for the downstream SCR system [8]. The DPF on BMW's diesel six-cylinder is combined with a NO_x storage catalyst, which can store barium sulfate, a product of combustion from sulfur additives in diesel fuel. The sulfur can be discharged at similar temperatures required for DPF regeneration [9].

Regeneration of the DPF is a function of temperature and accumulated soot mass. Manufacturers have resorted to alternative injection strategies and specialized coatings to achieve these high exhaust temperatures. The Audi V6 bi-turbo TDI uses coatings on the dual DPF canisters combined with a triple post-injection strategy designed to safely provide

enough heat into the exhaust system to trigger a regeneration event [6]. If there is enough temperature in the exhaust, it is possible to continuously regenerate the particles as they are trapped on the filter medium. An extreme case of such a system is found on the Audi R15 TDI entry for the 24 hours of Le Mans. In this situation minimal power loss is a key design goal, which translates to minimal exhaust back-pressure. The DPF used is designed in collaboration with DOW automotive, and results in constant regeneration above 650 degrees Celsius, with temperature capability of 1000 degrees Celsius and higher, as found in the racing environment. The DPF does not exceed the design goal of 200mbar of back pressure during normal racing conditions [10].

Selective Catalytic Reduction of NO_x

Manufacturers have had to resort to aftertreatment systems to meet the mandated levels of NO_x emissions. In an SI engine, the tailpipe NO_x emission level is kept low by the use of a three-way catalyst (TWC) and an exhaust air-fuel ratio (lambda) control strategy. Optimum operation of the TWC, however, requires constant switching between excess oxygen and excess hydrocarbon. In a CI engine, this is not practical, since the exhaust typically carries excess oxygen. Therefore, on a diesel engine, the preferred method of accomplishing the reduction of NO_x is the Selective Catalytic Reduction system, or SCR. Different types of SCRs have made their way into both heavy duty and light passenger diesel vehicles, however, each individual method has its advantages and drawbacks. The following subsections will discuss three viable SCR methods.

AMMONIA INJECTION

Ammonia (NH_3) on its own is highly toxic and has a high vapor pressure. It must be transported in high-pressure containers and is unfit for use in highway vehicles. Aqueous ammonia is much less toxic and can be safely transported; therefore it is suitable for use as a reductant for highway diesel vehicles. In ammonia SCR systems, the primary reaction by which NO_x is reduced may be described as

$$4NO + 4NH_3 + O_2 \rightarrow 4N_2 + 6H_2O. \quad (1)$$

Since the primary component of NO_x emissions in diesel engines is NO, which typically forms 90% of NO_x emissions, this reaction is effective in reducing the overall tailpipe NO_x emissions. A faster reduction reaction occurs when the inlet exhaust gas contains nearly equal parts of NO and NO_2, however, an inlet gas containing primarily NO_2 results in a slower reduction reaction [11]. Due to the toxicity of NH_3, it is undesirable to have any amount of ammonia slip post-catalyst. Ammonia slip can be caused by injecting ammonia into the SCR at high ratios and typically decreases with increasing temperatures. Stationary SCR applications are regulated to a maximum of 5 to 10vppm, which is typically unnoticed by smell [4]. Ammonia slip can be safeguarded against by installing an oxidation catalyst downstream of the SCR, which adds cost and complexity to the aftertreatment system.

The first application of ammonia SCR on a mobile application was in 1990 on an 8MW two stroke diesel marine engine. The system was designed to reduce 92% NO_x to comply with restrictions on outlet NO_x concentration in certain ports. The system was also equipped with a bypass for unrestricted areas [4]. Recently, injecting gaseous ammonia has been proposed as a way to obtain better low-temperature SCR performance. The advantage over liquid injection is better mixing and better low temperature performance, but implementation would require costly high pressure tanks and plumbing [12].

UREA INJECTION

Urea based SCR systems have received the highest level of acceptance as a mobile NO_x reduction solution. Urea ($CO(NH_2)_2$) will hydrolyze with water in high temperature environments to ammonia and carbon dioxide. For this reason, a water solution of urea is a non-toxic alternative to delivering the ammonia required for SCR NO_x reduction. The method through which urea decomposes and hydrolyzes to ammonia may be described as

$$CO(NH_2)_2 \rightarrow 2NH_2 + CO \quad \text{and} \quad (2)$$

$$CO(NH_2)_2 + H_2O \rightarrow 2NH_3 + CO_2, \quad (3)$$

respectively. Once the ammonia has been generated, the reduction process follows Equation (1). The first mobile application of urea injection for SCR NO_x control was on a ferry system

that travelled between Sweden and Denmark in 1992 [4]. Since then, there have been many more applications of urea injection, including production passenger vehicles.

Urea injection comes with a few challenges when applied to the mobile vehicle exhaust. One of the main problems is freezing of the stored urea. Since urea has a freezing point of -11 degrees Celsius, special equipment is required in the delivery system to prevent freezing in the on-board storage tank. Volkswagen addressed this problem on the 2011 2.0l TDI engine by using a combination of a tank heater with temperature sensor and insulation, removal of the urea solution from the lines upon engine shut-down, and a heated metering line. Combined with computer control of the heating elements, the system is capable of operating in temperatures below 0 degrees Celsius [8].

Before urea injection was implemented in production vehicles, one of the concerns was enforcement. In other words, an enforcement program had to be established to ensure that operators do not let the on-board urea tank become empty. A proposed solution was to have a dual nozzle for refueling the diesel and urea on the vehicle simultaneously, eliminating the need for the operator to remember to refill the urea storage tank [4]. Such a system would require a large implementation cost, and naturally has not become the preferred solution for current vehicles. Passenger vehicles equipped with urea SCR systems typically have their urea storage tanks replenished during the routine oil service. A urea level sensor on Volkswagen TDI vehicles is tied into the on-board diagnostics system (OBDII), emitting a maintenance warning if the urea needs to be refilled [8]. It is also possible for the operator of these vehicles to replenish the urea by means of commercially available products such as BlueDEF, or similar. Certain vehicles' on-board diagnostics systems will limit available engine torque or vehicle speed when the urea tank needs to be refilled as an incentive to keep the system filled [13].

Although urea injection is a non-toxic alternative to ammonia injection, both systems suffer the same problem of ammonia slip. This occurs when more reductant is injected than the catalyst can use to reduce NO_x emissions. One solution to this problem is the oxidation catalyst, as mentioned before. A more targeted approach to solving the problem is through the use of a feedback signal to control the amount of reductant injected onto the catalyst. The use of a NO_x sensor provides a direct feedback signal of the emission that is being reduced. The current Mercedes-Benz BlueTEC and Volkswagen TDI aftertreatment systems

use a NO_x sensor for diagnostics and control of the urea injection system. The TDI system compares the measured NO_x at the outlet of the catalyst system with a model estimate of the NO_x concentration at the inlet of the catalyst to determine SCR health [8]. Advanced control strategies have been explored around the use of a NO_x sensor, with results showing a maximum of 10ppm ammonia slip while maintaining a NO_x reduction of 92% over a simulated EPA UDDS[2] [14]. Delphi developed an ammonia sensor and a control algorithm to demonstrate its robustness to urea delivery perturbations and ability to adapt to catalyst aging. Using the ammonia sensor, a NO_x reduction target of 90% was maintained despite a 30% disturbance in urea injection. Ammonia slip was maintained at a maximum of 31ppm during the 30% urea disturbance under ammonia sensor control, compared to a maximum of 83ppm under NO_x sensor control. The work by Delphi describes that the primary advantage in using an ammonia sensor over a NO_x sensor is lower ammonia slip and better transient performance, due to the cross-sensitivity problems of currently available NO_x sensors [15].

An interesting approach to achieving fast light-off of the catalyst is the use of a reduced size primary catalyst in conjunction with an appropriately sized secondary catalyst. Volkswagen uses such a system with claims that the NH3 reductant is more evenly distributed over the second catalyst.

HYDROCARBON INJECTION

In a hydrocarbon (HC) based SCR system, a hydrocarbon is injected on the catalyst to selectively reduce the NO content of the incoming exhaust. This system has advantages over Urea and Ammonia, when used in mobile applications, in that diesel fuel may be used as the hydrocarbon, thus eliminating the need to carry and refill another on-board fluid. These types of systems have been referred to in literature as "active deNO_x catalysts" and "lean NO_x catalysts." Hydrocarbons may be supplied by utilizing post injection on the common rail system, or by installing an additional injector [4]. The chemical reaction taking place in an HC deNO_x system may be described as follows,

$$NO + Hydrocarbon + O2 \rightarrow N2 + CO2 + H2O. \quad (4)$$

[2] Urban Dynamometer Drive Schedule (UDDS)

As with the previously described SCR systems, the HC based system has a few drawbacks. Achieving an optimum temperature is critical for useful NO_x reduction, however, due to the exothermic nature of injecting HC, over-injection of the reducing HC can drive the catalyst temperature past that of optimum NO_x reduction. During over-temperature conditions the reductant can oxidize before reaching the catalyst, reducing its effectiveness in reducing NO_x [16]. The catalyst also has what is known as a light-off temperature, which describes the minimum temperature required for significant NO_x reduction. This optimal temperature operating range has been described in literature as the "catalyst window" [4]. Space velocity is defined as the volume of reactant gasses flowing through the catalyst per hour divided by the volume of the catalyst [17][18]. This may be expressed as

$$Space\ Velocity = \frac{Flow_{SCR}}{Volume_{SCR}}, \tag{5}$$

where $Flow_{SCR}$ represents the volumetric flow through the catalyst and $Volume_{SCR}$ represents the volume of the catalyst. In dealing with SCR systems, NO_x reduction has been shown to decrease with increasing space velocity [19], which can lead to very large-sized catalysts depending on the formulation of the catalyst. Space velocities can vary from 10,000 h^{-1} to 300,000 h^{-1} when dealing with catalysts, with 50,000 h^{-1} being a typical value for a well-sized cost-effective system [4] [20].

Hydrocarbon slip becomes a problem on this type of catalyst, since HC is a harmful emission, and any HC that is unused in reducing emissions or propelling the vehicle results in wasted fuel. An oxidation catalyst can be used in this case (as with the ammonia based SCR system) to oxidize any unused HC that exits the catalyst. It has been found that HC-SCR systems are adversely affected by the presence of H2O in the inlet gas, and the type of hydrocarbon used as the reductant has an effect on the possible NOx reduction [16]. As shown in Equation (4), oxygen is required to reduce NO to N2. It has been found that optimal NO reduction occurs when the ratio of HC to oxygen is closest to the stoichiometric ratio required for complete HC oxidation [21]. As with ammonia and urea systems, in HC based SCR systems, precise control of the injected HC is critical to obtaining the best NO reduction with minimal HC slip.

A combination HC and Ammonia dual-SCR system has been tested, in which HC is injected on to the first catalyst, reducing NO_x and simultaneously forming ammonia to act as

the reducing agent for the second NH_3-SCR. The dual system has the advantage of not requiring the use of precious metals, while being able to reduce up to 95% of the incoming NO_x emissions. This system is proposed for use in light duty vehicles where exhaust temperatures are relatively low [20].

Previous HC-SCR Modeling Work

Reduction of NO_x emissions by hydrocarbon injection has received limited attention in terms of modeling the catalyst behavior for use in transportation applications. The following paragraphs will review some of the previous work that applies to SCR modeling and its relevance to the current work.

A study of a diesel aftertreatment system describes a multi-bed system comprised of an SCR upstream of the injector and three HC-SCR beds downstream of the diesel injector [22]. Diesel exhaust is produced by a 6.7l Volvo diesel engine. In the study, gas analyzers are set up to sample exhaust gas at the point of injection and after each of the first two downstream catalyst beds. Temperature is measured with thermocouples located at the same points as the gas analyzers. During experiments, engine load is used to vary temperature in the catalyst. A 30 second pulse of reductant (diesel) is injected every two minutes during transient and steady state experiments.

The thermodynamic and chemical processes occurring between each sampling point is modeled as ten stirred tanks in series. The model is first fitted to the experimental data by using the inlet measurements (at the injector) as the known input to the system and fitting the model to the measured values at the outlet of the first HC-SCR. The model is also fitted by using the measurements at the outlet of the first HC-SCR as the input of the system and fitting the model to the measured values at the outlet of the second HC-SCR.

The model developed in the study is reasonably accurate in predicting outlet NO_x concentration, as well as CO and NO_2 concentrations. This model is primarily used to characterize the system as a whole, taking into account flow rates and multiple simultaneous chemical reactions. This approach is sensitive to the chemical composition of the diesel fuel used as a reductant. Non-homogeneous temperature distribution through the catalyst also affects performance of the model, since the data used for fitting measures gas temperatures

outside of the catalyst. Furthermore, this model does not take into account the typically poor NO_x reduction that is typical of HC-SCR in the low temperature operating range.

Although this model provides an overall description of the reactions taking place through the catalyst, in the current work, the primary goal is to reduce NO_x. Thus a model which focuses on the relationship between inlet NO_x, temperature and injected Hydrocarbon is more desirable.

In a different study, a statistical model of a HC-SCR system is generated from experimental data [23]. Data obtained from a single cylinder naturally-aspirated direct injection experimental diesel engine displacing 0.773 liters was fitted with a reformed EGR system and a HC-SCR system. The HC-SCR system used in the study does not include an upstream exhaust injector to provide hydrocarbon to the SCR, as in the current work. Testing was performed within an operating range of 0-30% EGR, 1200-1500 RPM and 25-50% engine load.

Using a statistical analysis, it was found that engine speed had the least influence on the percentage of NO_x reduction across the HC-SCR. Engine load was found to have the highest effect in conversion efficiency, causing better efficiency at higher loads. This is attributed to higher loads generating optimal temperature conditions for the HC-SCR. The statistical model of the HC-SCR is described mathematically as

$$\begin{aligned} Conversion\ \% = {} & 19.33 + 54.3EGR + \\ & 84.1 \propto -18.78EGR^2 - 52.89EGR \cdot \alpha, \end{aligned} \tag{6}$$

where α is the engine load.

Although the statistical model of HC-SCR is useful in analyzing the key factors influencing NO_x conversion efficiency, the model has limited use in terms of implementation for a control or diagnostic system. Since this system is analyzed without the use of an upstream hydrocarbon injector, temperature effects can be related back to engine load. Thus the model is unsuitable for injected HC-SCR systems where exothermic reactions in the catalyst can occur independently of engine load.

CHAPTER II: EXPERIMENTAL METHOD

Description of Test Equipment

Tests were performed at the engine test cell in the Texas Diesel Testing and Research Center located at the University of Houston. The engine was a Cummins "N14" marine diesel engine displacing fourteen liters, rated at a maximum torque of 1653 lb.-ft. at 1400 rpm. Specifications are shown in Table 1.

Table 1: Cummins N14-M Specifications.

Manufacturer	Cummins
Model	N14
Features	EGR, Turbocharged
Number of Cylinders	6
Displacement	14 liters
Compression Ratio	17.0:1
Rated Power	360 HP @ 1800 RPM
Maximum Torque	1219 lb.-ft. @ 1400 RPM
Exhaust Flow	2070 CFM
NO_x Emissions[3]	5.97 g/bhp-hr
HC Emissions	0.12 g/bhp-hr
CO Emissions	0.68 g/bhp-hr

The engine served to generate exhaust under fixed throttle and fixed engine speed, with the aftertreatment system being the primary focus during the testing. The exhaust gasses are taken from the outlet of the turbocharger, and then split into two pipes which are fed into the DPF. From the DPF, the two pipes are joined back into one and then fed into the inlet of the SCR. A bypass runs from the inlet of the SCR to the outlet, to allow the operator to control flow through the SCR independent of engine conditions during testing. The complete exhaust system is shown in Figure 4 below.

[3] Emissions measurements taken under ISO8178 Cycle E3 standards

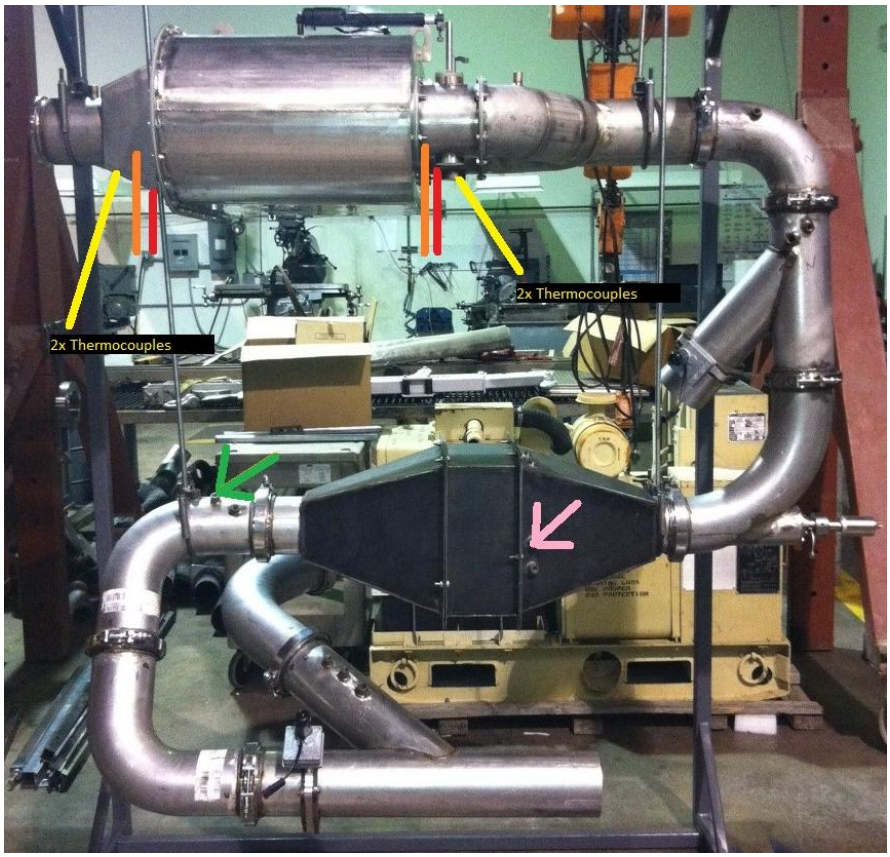

Figure 4: Diesel aftertreatment system including DPF and SCR, with injector and flow bypass.

In Figure 4, exhaust enters the DPF (shown at the top of the image), and exits after the SCR (shown at the bottom of the image). The injector can be seen in one of the test positions located on the 90 degree elbow pointing into the inlet of the SCR. The bypass takes exhaust from upstream of the injector on the vertical pipe, and combines with the exhaust flow at the outlet of the catalyst on the horizontal pipe shown in Figure 4. The flow through the bypass and SCR is adjusted via two electronic valves, one on the bypass, and one on the outlet of the SCR.

The catalyst is composed of four cubic bricks, each measuring six inches on any edge, arranged together to form a rectangular prism measuring 12 inches tall by 12 inches wide, and six inches in the direction of the exhaust flow. Eight Thermocouples are placed inside the catalyst in various positions, as shown in Figure 5.

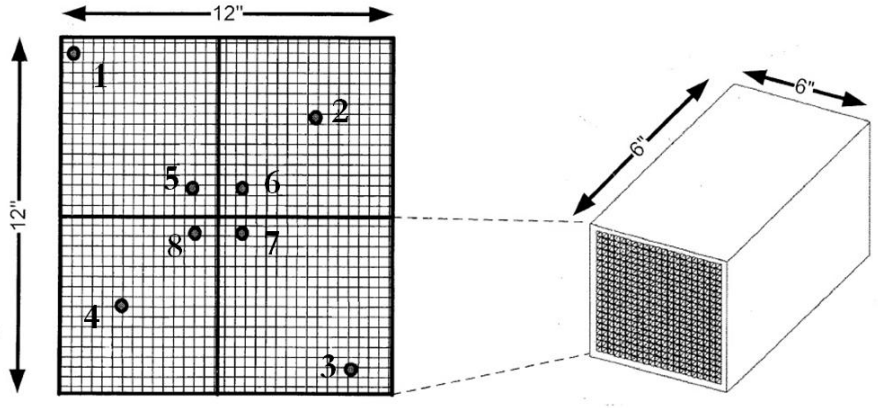

Figure 5: Locations of thermocouples on SCR and individual brick geometry.

In Figure 5, the thermocouples are placed at various depths from the front face of the catalyst. This was done to obtain internal catalyst temperatures at different distances away from the axis parallel to exhaust flow, and away from the injector. The SCR and the piping leading up to the SCR is covered with insulating blankets to prevent convective cooling of the exhaust and to attempt to maintain an even temperature distribution inside the catalyst. The following table summarizes the installation depths of the thermocouples.

Table 2: Thermocouple depth in catalyst

Thermocouple Number	Distance from front face
1	3”
2	3”
3	2”
4	4”
5	4”
6	5”
7	2”
8	3”

Flow through the catalyst is calculated by taking air consumption (AC), which is measured using a hot wire anemometer at the intake, and subtracting “Flow Pitot” which measures the exhaust bypass flow. “Flow Pitot” is calibrated by opening the bypass valve so that 100% of the exhaust flow is being bypassed, and then adjusting the value of “Flow Pitot” to match the AC value. This method provides an approximation of flow through the SCR, and more importantly, provides a method to compare SCR flow between tests.

An ultrasonic injector is used to deliver hydrocarbon to the SCR in the form of commercially available diesel fuel. Where normal injectors use high liquid pressures and small orifice diameters to achieve fine atomization, the ultrasonic injector uses an ultrasonically vibrating device near the orifice to pump the diesel out of the injector at high velocities, thus creating a finely atomized mist. The ultrasonic injector comprises of a control box, a pump and fluid reservoir, a solenoid valve, and the injector itself. The control box contains the electronics necessary to drive the ultrasonic injector nozzle, and provides a central location for power distribution. The pump and fluid reservoir contains the diesel fuel being injected, and provides the ability to provide a delivery pressure to the injector from 600 to 1200 psi, adjustable via a pressure regulator. The solenoid valve is plumbed in just before the injector in the pressurized supply line and its position determines if fuel will be supplied to the injector. The injector is supplied with compressed air for cooling of the electromechanical components driving the ultrasonic mechanism. Flow rate through the injector is possible by manually changing the nozzle orifice, adjusting the supply line pressure, or adjusting the ultrasonic amplitude. The ultrasonic amplitude may be adjusted infinitely between 50% and 100%.

Controlling the injector on and off events is accomplished through a National Instruments (NI) highly configurable Compact RIO programmable logic controller (PLC). The Compact RIO (CRIO) PLC consists of a chassis that accepts modular input/output cards that are capable of measuring and outputting different types of signals. For use with the injector system, the CRIO is fitted with an NI 9481 relay card, which is capable of switching 30 dc volts at one ampere, which is used to switch the solenoid valve attached to the supply line of the injector. Using LabView, it is possible to supply a square wave signal to the switching output on the NI 9481 card, making it possible to turn the injector on and off at various duty cycles and periods. An analog to digital input card (NI 9205) allows inputs of +/- 10 dc volts from sensors and other equipment. This allows for closed loop operation of the injector when connected to a NO_x signal.

The exhaust gas pre and post SCR is sampled and measured by a Fourier transform infrared (FTIR) spectroscopy gas analyzer, connected to an AVL data acquisition system running Puma software which records the signals at a frequency of 10hz. Table 3 shows the relevant signals that are captured for analysis.

Table 3: Description of recorded variables

Signal name	Description	units
Conc_CO_SCRin	SCR inlet CO	PPM
Conc_CO_SCRout	SCR outlet CO	PPM
Conc_NOX_SCRin	SCR inlet NO_x	PPM
Conc_NOX_SCRout	SCR outlet NO_x	PPM
Conc_THC_SCRout	SCR outlet Total Hydrocarbons	PPM
FlowSCR	Estimated volumetric flow rate through SCR	m^3h^{-1}
InjectorON	Injector on signal	unitless
TORQUE	Engine Torque	N-M
T_CHAN21-T_CHAN28	Thermocouples 1-8	Celsius
time	Time	Seconds

Experimental Method

The objective of testing the SCR is to obtain enough data to model the NO_x reduction efficiency at various operating conditions. An operating condition is defined as a different point in flow rate and temperature. Flow rate has an effect on the reduction efficiency because this value dictates the amount of time that the exhaust spends in the SCR (space velocity). High catalyst temperature is required for the reduction reaction to take place, and thus the NO_x reduction is temperature dependent. It is desirable to create tests which capture the dynamics of the catalyst over a wide range of flow rates and temperatures to produce accurate models.

Typical tests would begin by choosing one of two available injector nozzle diameters. The two different orifice diameters of the injector nozzles were 0.003 inches and 0.005 inches. These diameters were selected based on documentation provided by the manufacturer

showing that the maximum flow rate of liquid through the ultrasonic nozzle can be achieved using the 0.005 inch diameter nozzle. The 0.003 inch diameter orifice was used in situations where slightly less fuel delivery was required. Once the orifice diameter was selected the next step was to adjust the pressure to the injector. Over all of the tests, this value was typically set to 800 psi, although 1200psi was explored. As expected, the primary effect noticed while changing the supply line pressure to the injector was that the fuel delivery rate changed.

Once the injector settings were adjusted, the engine would be brought up to the typical operating point of 1200 RPM and 35 percent throttle. By locking down the throttle position and choosing a setpoint engine speed, the engine dynamometer automatically applied as much load as needed to maintain the setpoint engine speed. For an engine speed of 1200 RPM and 35 percent throttle, the engine torque typically varied between 1200 and 1300 Newton-meters. A histogram of this variation over a complete test lasting 105 minutes is shown in Figure 6.

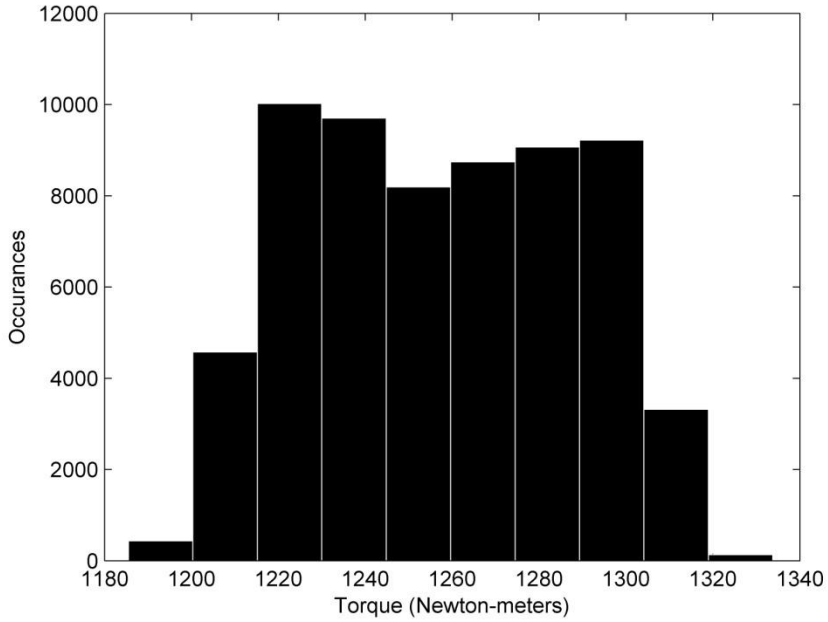

Figure 6: Histogram showing variation in engine torque.

After establishing stable engine operation, the catalyst bypass flow is adjusted for the desired volumetric flow rate through the catalyst. Unlike the torque signal, flow through the SCR demonstrates a very steady average value, with only slight variations about the mean. For

example when attempting to set the SCR flow rate to a value of 200 m^3h^{-1}, a mean value of 204 m^3h^{-1} is observed, with a bell-curve variation between 175 and 240 m^3h^{-1}. This behavior can be seen in Figure 7 below. By comparing Figure 6 and Figure 7, it is clear that the oscillations in engine torque do not affect the volumetric flow rate of the exhaust.

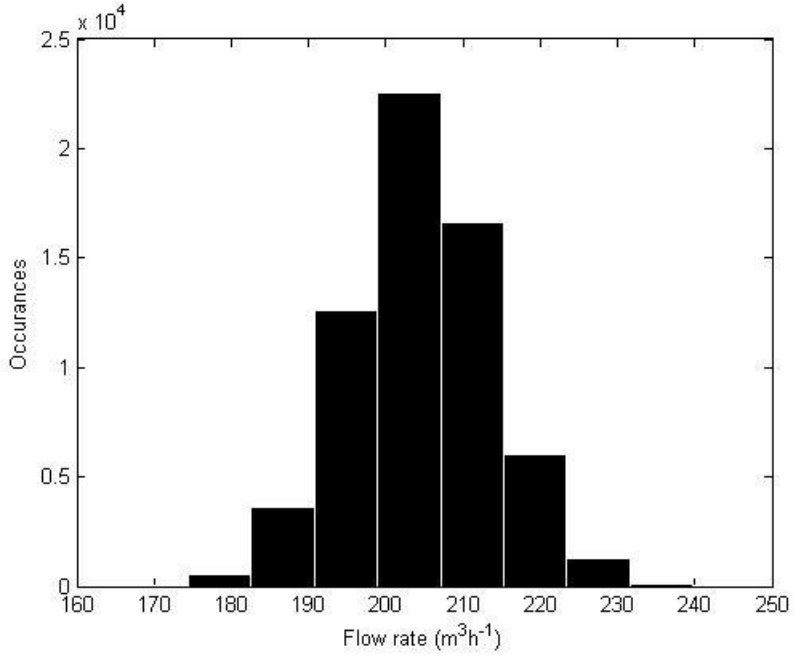

Figure 7: Histogram showing variation in SCR flow

Once the catalyst flow is set to the desired value, the engine is allowed to reach steady state meaning that the catalyst internal temperatures are constant, and at least 300 degrees Celsius. At this point, a pre-determined test plan would be carried out in which the injector would be turned on and off with all other operating conditions remaining as set. As detailed previously, the user may select the duty cycle and period of the injection event. During a test, typically the period is fixed and the duty cycle is varied. This allows the catalyst to undergo a variety of temperatures caused by the exothermic nature of the HC-SCR interaction, and a variety of NO_x reduction levels as a result of varying injector duty cycle.

CHAPTER III: ANALYSIS

Basis for Modeling Approach

The method of modeling found in the following sections is inspired by the work accomplished on an automotive three-way catalyst (TWC) system [24]. This work demonstrates a method of measuring catalyst health by comparing the concentration of the inlet oxygen against the concentration of oxygen at the middle of the TWC to calculate an adaptive gain value K_{TWC}. The K_{TWC} is defined as

$$\dot{V}_{HEGO}(i) = K_{TWC}\Delta\varphi(i), \tag{7}$$

where $\dot{V}_{HEGO}$ refers to the voltage of the narrowband oxygen sensor mounted at the middle of the catalyst, and $\Delta\varphi(i)$ refers to the changes in fuel-air ratio of the gas entering the catalyst. Defined as in (7), K_{TWC} represents the inverse level of oxygen storage capacity (OSC) in the catalyst. It is found that as a catalyst ages, its ability to store oxygen diminishes and incidentally, K_{TWC} values tend to increase. On a fresh catalyst, high OSC results in a low K_{TWC} value.

The K_{TWC} gain method works particularly well on TWC systems combined with SI engines, because the oxygen content of the exhaust before, inside, and after the catalyst strongly correlates with the mechanisms through which the harmful outlet emissions are minimized. This can be seen in the primary chemical reactions for the TWC, shown in (8), (9), and (10), as follows:

$$NO_x \rightarrow O_2 + N_2, \tag{8}$$

$$CO + O_2 \rightarrow CO_2, and \tag{9}$$

$$C_xH_y + O_2 \rightarrow CO_2 + H_2O. \tag{10}$$

In the above set of equations, (8) describes the reduction of NO_x to nitrogen and oxygen, (9) describes the oxidation of CO to CO_2, and (10) describes the oxidation of hydrocarbon to carbon dioxide and water. Oxygen plays a key role in each of these reactions. It is known that low oxygen content (rich condition) at the inlet of the catalyst implies high hydrocarbon content and carbon monoxide, while high oxygen content at the inlet (lean combustion)

implies an exhaust that carries with it a high NO_x concentration [1]. Thus, by comparing the inlet and outlet oxygen concentrations, it is possible to generate a value which describes how effectively the three simultaneous reactions are taking place within the TWC. Furthermore, high oxygen levels sensed at the middle of the catalyst implies either a deficiency in the oxidation reactions, or a healthy reduction of NO_x. From this brief overview of the chemical reactions driving the TWC, it is possible to see why the OSC is useful when establishing a model for the health of a TWC working on an SI engine.

When dealing with a CI engine, the K_{TWC} approach does not apply directly, due to the excessive oxygen content of the exhaust gasses, specifically, $\Delta\varphi(i)$ will not represent deviations from the unity fuel-air ratio as in the case of the SI engine. Furthermore, the narrow-band oxygen sensor used for sensing oxygen levels mid-cat will not provide a useful reading since it will almost always sense a lean condition (excessive oxygen) relative to stoichiometry when placed in the diesel exhaust. Simply converting the oxygen sensor based adaptive gain to a NO_x sensor based adaptive gain approach for use in an HC-SCR system is not sufficient to determine catalyst health because the NO_x value at the SCR inlet does not relate to the hydrocarbon content being brought to the catalyst, as in the oxygen based adaptive gain. In a NO_x based adaptive gain, the SCR inlet NO_x value could be constant while the SCR outlet NO_x value could be fluctuating widely due to unperceived (by the inlet NO_x sensor) hydrocarbon injection. It is necessary to take into account the amount of reductant being injected and how that reductant interacts with the catalyst to accurately estimate the health of the catalyst. By knowing the inlet NO_x value and the injected amount of reductant, and assuming excess oxygen, the left side of (4 is complete, and it is possible to estimate the outlet NO_x of the healthy system after applying corrections for space velocity, and temperature. This forms the basis for the model described in the next sections.

Development of the HC-SCR Model

The model for the HC-SCR system starts with the inlet NO_x value as an input. This is the reference value since any outlet NO_x must be equal to or lower than this value. A subtraction must take place which is representative of the conditions of the catalyst and the amount of fuel being injected to replicate the outlet NO_x signal from the inlet NO_x signal.

The temperature sensors are placed throughout the SCR in different locations, as shown in Figure 5. The delivery of fuel to the SCR is not uniform, which manifests itself as non-uniform temperature distribution in the HC-SCR system, especially during injection events. Figure 8 demonstrates this behavior during a test session.

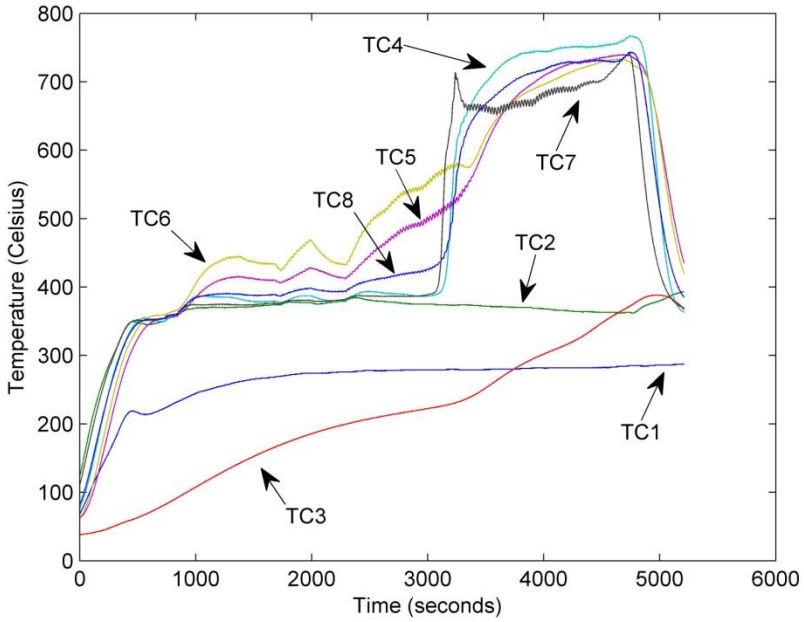

Figure 8: Internal temperatures during one test session.

In the above figure, there are five temperature signals that follow the light-off trend, while three of the temperature signals do not. The three signals that do not follow the light-off behavior are thermocouples 1, 2, and 3. These are placed near the outer edges of the catalyst, and closer to the front face of the catalyst, unlike thermocouple 4 which did demonstrate light-off behavior and was placed further from the front face, but similar to 1, 2, and 3, near the outer edge. Thermocouples 5, 6, 7, and 8 clearly demonstrate the light-off behavior of the catalyst, while thermocouple 7 demonstrates the greatest sensitivity to injection events. This can be easily explained by the shallow depth relative to the front face of the catalyst at which thermocouple 7 is placed. The most important thing to notice in Figure 8 is that the temperature distribution within the catalyst varies depending on the position of the temperature measurement.

During the test session, NO_x values at either end of the catalyst are recorded, along with several other channels. These are plotted below against temperature to demonstrate the temperature dependence of the catalyst on NO_x reduction.

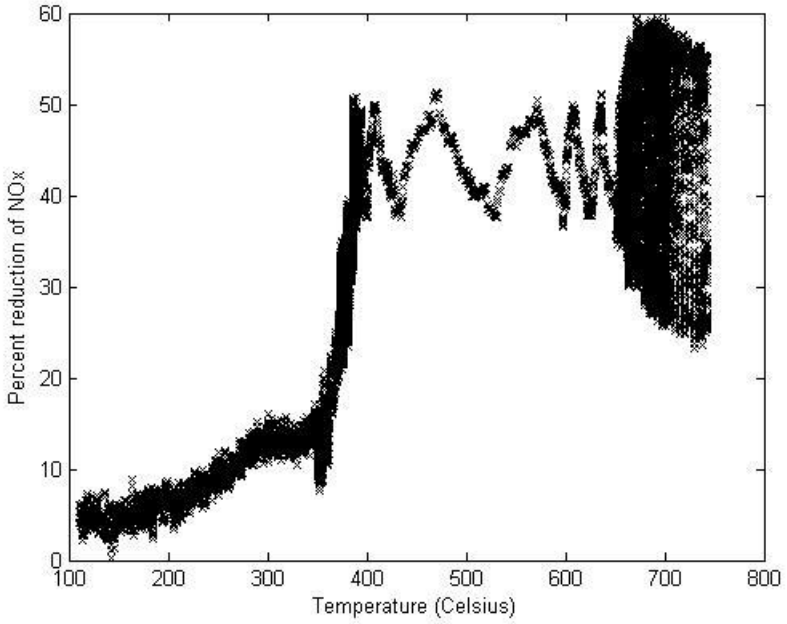

Figure 9: NO_x reduction vs. Temperature at space velocity 3108h^{-1}, average inlet NO_x 1700ppm.

In Figure 9 above, the concentration of NO_x at the outlet is divided by the concentration of NO_x at the inlet of the SCR and subtracted from one to produce a percent reduction. Time delay is not considered in this case since the inlet NO_x signal is essentially a constant, with slight noise about the mean. A light-off temperature is easily visible when examining the jump from 15% reduction to nearly 50% reduction. After reaching the light-off region (between 380 and 650 degrees Celsius) reduction remains constant as a function of temperature until reaching the temperatures higher than 650 degrees Celsius. At this point the quantity of fuel being injected onto the catalyst is the same or higher, and the percentage of NO_x reduction starts to show a downward trend. This behavior leads to a model that maps reductant injection effectiveness on reduction of NO_x as a function of temperature. Specifically, the function takes on the form of a non-linear temperature scaling factor with two adjustable parameters.

The fuel injector on off signal is a true binary signal taking values of one or zero (i.e. on or off). When plotted over time, this is a square wave; however, the output NO_x value does not resemble a square wave as shown in Figure 10.

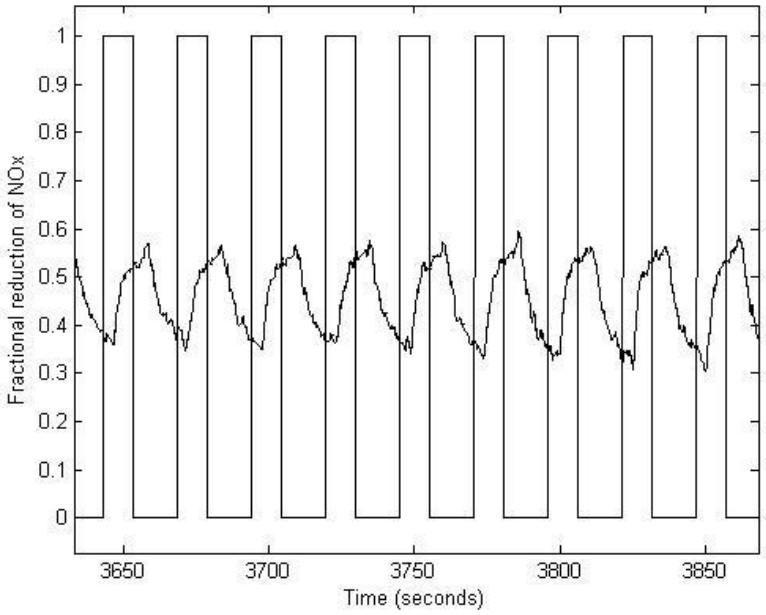

Figure 10: Comparison of NO_x and Injector signals over time.

To approximate the behavior of the outlet NO_x as a function of the injector signal, some modification to the injector signal will be required. The simplest method by which to do this is to apply a first order filter to the injector signal. The continuous time representation of the first order filter applied to the injector signal can be written as

$$G(s) = \frac{1}{\tau s + 1}, \tag{11}$$

where G(s) represents the Laplace transform of the output divided by the Laplace transform of the input. Using the first order filter gives the injector a shape that more closely resembles the outlet NO_x value, without adding overly complex dynamics to the signal. For instance, just having a first order filter rather than a higher order filter allows for simple adjustment of one value, τ, which represents the time constant of the first order system, whereas a higher order filter would have more complex dynamics to tune and optimize.

Although time delay was neglected when calculating the percentage of NO_x reduced, it is necessary to take the delay into account when developing a model to relate injection. Time delay in this case represents the transport delay from the onset of commanding diesel injection, to the time when NO_x reduction due to that injection is noticed. This transport delay is affected by space velocity, as higher space velocities will result in faster transport of the exhaust gasses from the inlet of the catalyst to the outlet. The transport delay is shown in Figure 11.

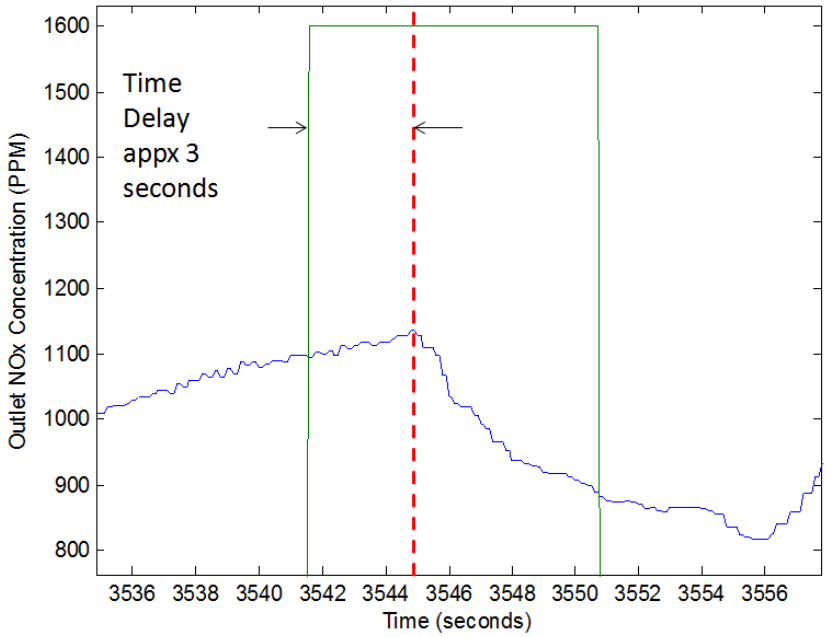

Figure 11: Outlet NO_x vs Time showing transport delay at space velocity of $3108h^{-1}$ during light-off activity.

In Figure 11, the injector signal has been multiplied by a constant to appear on the same scale as the NO_x outlet signal.

The final consideration to take into account in the model is the effectiveness of the injection event on the reduction of NO_x. This is similar to having a temperature factor; however, some parameter must compensate for injections on different space velocities at the same catalyst temperature. Such a parameter can be implemented in the model in the form of a gain, and the expectation is for this gain to become smaller with increasing space velocity.

Taking the above key characteristics into account is important when producing a model of the SCR system. In the next section the implementation of the model in a simulation environment will be described.

Description of HC-SCR Model

The HC-SCR model is created using the Simulink simulation environment within The Mathworks MATLAB software. The model has inputs of inlet NO_x, capability to handle three temperature signals (easily expandable to handle all eight), and the injector signal. From these input signals an estimate of the outlet NO_x is generated. The next few paragraphs will describe the model and each of its components. The Simulink representation of the model is shown in Figure 12.

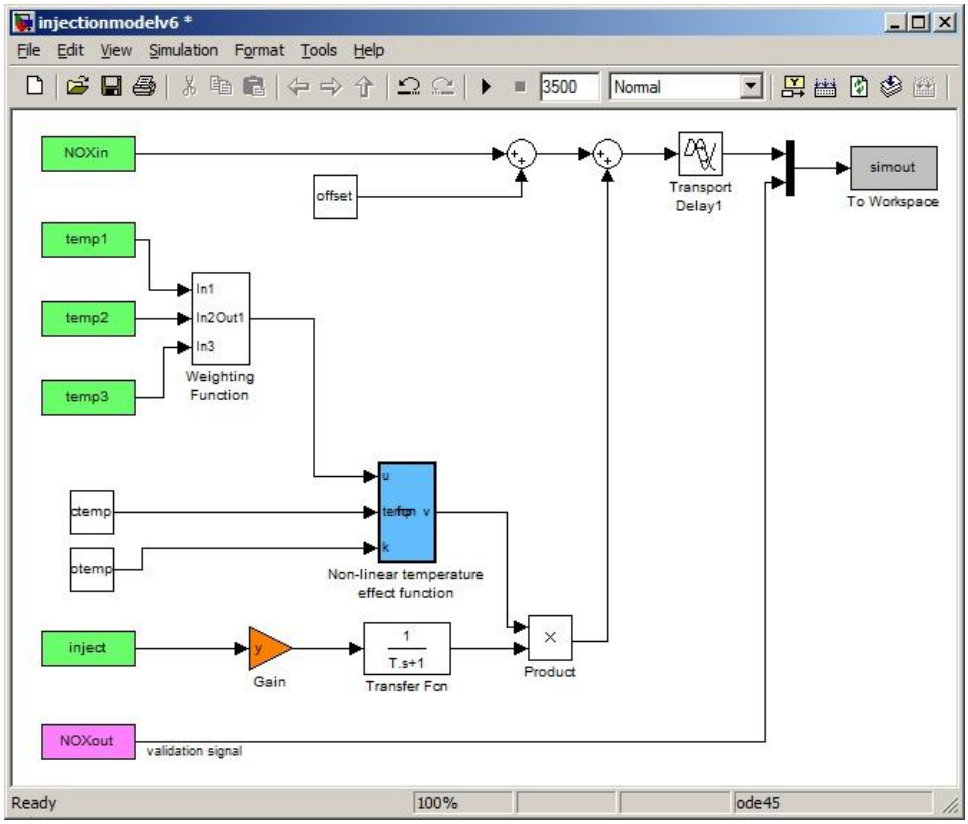

Figure 12: Simulink representation of model.

The inputs to the model, located in the upper left hand corner of Figure 12 are labeled NOXin, temp1, temp2, temp3, and inject. The output of the model can be found at the out

terminal of the block labeled Transport Delay1. From there it is multiplexed with the NOXout signal, for validation purposes and sent to the workspace where it can be plotted and analyzed. Each of the input signals are from experimental data captured at 10Hz, thus the output signal is also at 10Hz.

In Figure 12, the NOXin signal is modified by a summing node and a constant labeled offset. The offset constant accounts for a difference between the NOXin and NOXout signal under constant operating conditions, with no hydrocarbon being injected. This value may also make up for any calibration error in the FTIR analyzer.

The weighting function shown in Figure 12 is represented in Simulink as a subsystem that contains a weighting function to select the most influential temperature signal. This helps to accommodate the temperature distribution across and through the catalyst. The weighting function subsystem is shown below.

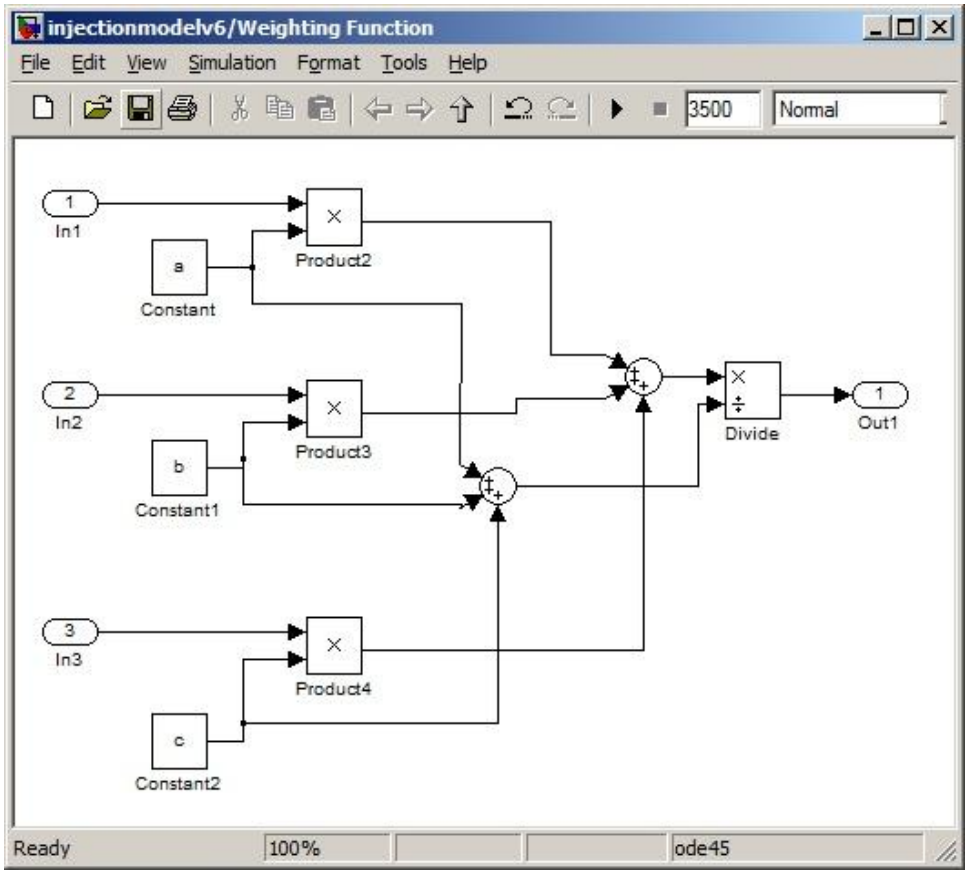

Figure 13: Weighting function subsystem.

Numerically, the output of the temperature weighting function can be described by

$$Temp(i) = \frac{aTemp1(i) + bTemp2(i) + cTemp3(i)}{a + b + c}, \qquad (12)$$

which can easily be expanded to include all eight thermocouples. By forcing the optimization software to only optimize these values, it is found that thermocouples which are placed closest to the center of the catalyst give the strongest correlation to NO_x reduction efficiency (i.e. the weighting coefficient is larger for thermocouple placed closer to the center). When allowing software to optimize the variables, values a, b, and c, are constrained to the interval [0,1].

The temperature value that is calculated from the weighting function is then put through the non-linear temperature effect function block. This block contains a non-linear function that can be described by

$$\begin{Bmatrix} for\ temp(i) < ctemp, & temp(i) = temp(i) \\ for\ temp \geq ctemp, & temp(i) = ctemp - k(temp(i) - ctemp) \end{Bmatrix}. \qquad (13)$$

The above conditional statement describes the non-linear function applied to temperature, which relates to the drop off of catalyst performance in over-temperature situations. The value "k" in Equation (13) is also referred to as "otemp," or the over-temperature coefficient, which is simply the slope of the drop off in the temperature function. This is also shown graphically in Figure 14.

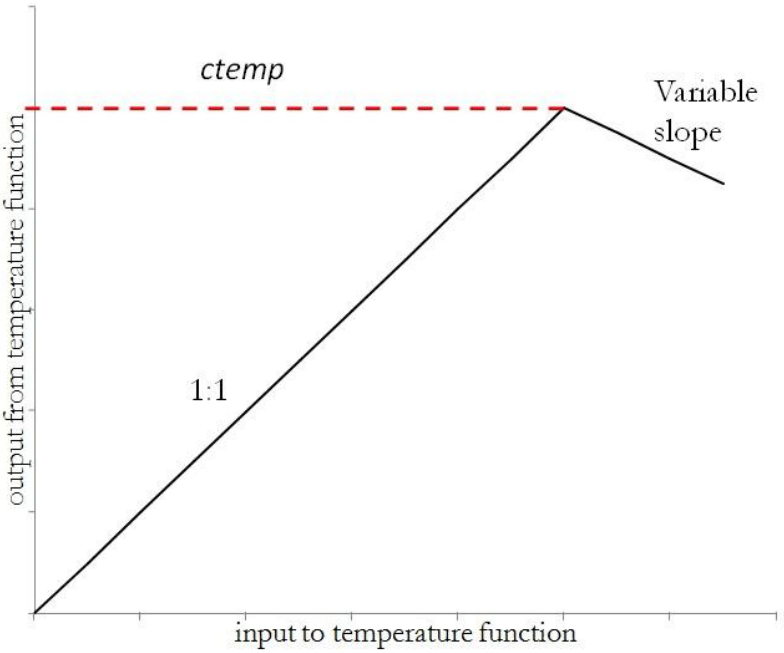

Figure 14: Output vs. input for non-linear temperature function.

During software optimization of the model parameters, the over-temperature coefficient is limited to the interval [-1,1]. Constraining this value as described significantly improves the convergence rate of all the model parameters.

The injector signal in Figure 12 is multiplied by a gain, "y." From there the value is passed through the first order filter labeled "transfer function" in Figure 12, to shape the signal from a square wave into more of a saw tooth wave, as previously described. (See Figure 10) The value produced by the non-linear temperature function is multiplied by the value that is produced by the first order filter to form a value to subtract from the offset inlet NO_x concentration. The signal that results gets put through a delay function, labeled "transport delay 1" in Figure 12. This block represents the transport delay that occurs when exhaust gasses carry the injected fuel from the inlet of the catalyst to the FTIR on the outlet of the catalyst. This value may be approximated by using the measured volumetric flow rate and the volume of the catalyst, as follows,

$$Delay = \frac{V_{SCR}}{Flow_{SCR}}, \tag{14}$$

where V_{SCR} is the catalyst brick volume, and $Flow_{SCR}$ is the volumetric flow rate through the catalyst. In this specific case, the catalyst volume is $1.41 \times 10^{-2} m^3$. Dividing this value by the SCR flow rate, in units of $m^3 h^{-1}$, results in a delay value in terms of hours. This may be multiplied by the constant conversion factor of 3600 to obtain the estimated delay time in seconds. Typical values for the delay time are shown in the following table.

Table 4: Estimated delay time based on flow rate.

Flow rate (m^3h^{-1})	Estimated Delay time (seconds)
44	1.16
165	0.31
204	0.25
333	0.153

The signal that results from the transport delay block is the estimate of NO_x at the outlet of the catalyst, based on inlet NO_x, temperature, and injection signals. A discrete time representation of the complete model may be written as

$$NOx_{out}(i+d) = NOx_{in} + C_1 + [f(temp(i)) \times (C_2 inj(i) - C_3 inj(i-1))]. \quad (15)$$

In Equation (15), the constant C1 serves the same function as the offset block in shown in Figure 12. Constants C2 and C3 combined with the current and previous sample of the injector signal represent the first order filter as well as the "y" gain of Figure 12. The temperature function is represented as $f(temp(i))$, with f defined as the conditional statements in Equation (13).

Calibration of Model

The model structure is established in such a way as to capture the key dynamics of the SCR by using parameters related to chemical and thermodynamic behavior of the catalyst. The parameters of the model are calibrated to previously acquired data using an optimization algorithm described in the following paragraphs.

Model parameters are calibrated to data sets using the Parameter Estimation tool box within Matlab's Simulink simulation environment. This tool box allows the user to apply three[4] different optimization methods to reduce either the sum of the squared errors (SSE) or the sum of the absolute errors (SAE) between the model generated estimation and the

[4] A fourth method, Pattern Search, is available but not included in this author's software package.

measured signal. The three different optimization algorithms available are simplex search, gradient descent, and non-linear least squares.

The Simplex search method within the Parameter Estimation tool box calls the embedded MATLAB function "fminsearch" which is capable of finding the minimum of a function of many variables without having to compute derivatives. The function "fminsearch" uses the Nelder-Mead Simplex algorithm. When applied to the proposed SCR model, this method requires little time to compute each iteration, but requires several iterations to arrive at a suitable solution. During attempts to estimate parameters for the SCR model, up to 400 iterations were completed before converging to a reasonable solution. This method is not used for the final optimization because it is not possible to place constraints on the model parameters being optimized. Having constraints on the model parameters helps to avoid situations where the parameters are completely out of feasible range (for example both negative and positive temperature weighting factors in one solution) and the estimated output matches the measured output with little error.

The gradient descent method within the Parameter Estimation tool box calls the embedded MATLAB function "fmincon" and performs a gradient descent optimization, also known as a steepest-descent optimization. This method works by computing the gradient around a point within the feasible region, and selects the next point in the direction of the steepest derivative that will minimize the function. The feasible region is defined by the constraints placed on the parameters. In the Parameter Estimation tool box, the gradient is calculated using a finite difference method, which may be improved upon by selecting to use a refined finite difference method which helps to eliminate noise in the gradient calculation. When used to estimate SCR model parameters, the gradient descent method is found to take a relatively long time to compute each iteration, with the parameters converging to a solution within 10 or less iterations. This method is sensitive to initial conditions, since there are several local minima and the initial guesses of the parameters could have a steepest descent direction that leads to a local minimum defined by incorrect model parameters. With the long iteration time and possibilities of incorrect parameter estimation, this method is not the preferred optimization method for calibrating the SCR model parameters.

The final method explored is the non-linear least squares method. This method calls the embedded MATLAB function "lsqnonlin" and uses a trust-region reflective algorithm.

This algorithm works by creating a quadratic Taylor series model of the function to be minimized around the initial guess point. The algorithm will specify a region in which to trust this model, and will only take a step within the trusted region around the point. As the algorithm proceeds and the model proves to be accurate through the steps, the trusted region will be increased. The trust region will be decreased if the Taylor Series approximation does not accurately model the original function. This method can initially be slower than Newton's method, but if the trust region can be made large, higher rates of convergence are possible [25]. When applied to the SCR modeling problem, this method is the quickest, typically converging within 15 minutes and 50 or less iterations when using the full sampling rate of the data (faster when using downsampled data) and is not as sensitive to parameter initialization as the other methods. Because the non-linear least squares method works best with the SCR modeling problem, it is selected as the primary method for estimating the model parameters for various data sets.

The model parameters are allowed to be optimized using the non-linear least squares method in the parameter estimation toolbox, with constraints placed on the temperature weighting factors, as well as the over-temperature factor. All other values are left unconstrained. Goodness of fit is done by using the sum of the square errors during optimization. During analysis, the average absolute error (AAE) is used. This may be computed as

$$Error = \frac{\sum_{i=1}^{n} NOxEst(i) - NOxActual(i)}{n}. \quad (16)$$

In the above equation, n represents the number of data points being analyzed, NOxEst is the estimated outlet NO_x concentration, and NOxActual is the measured outlet NO_x concentration. Both model parameters and graphs showing the estimated data and measured data are shown in the first section of the appendix.

CHAPTER IV: VALIDATION OF MODEL

Validation Over Different Data Sets

To show that the model captures the dynamics of the system, model parameters calibrated for one data set are applied to others taken at similar flow rates. Other data sets might have different injection period and duty cycle, as well as different temperature distribution and temperature history. In cases where different data sets are not available at similar conditions, the first half of a data set may be calibrated and validated against the second half.

The model parameters are calibrated for the second data set acquired on 12/6/2011. This data set demonstrates a wide range of temperatures at a constant volumetric flow rate of $43 m^3 h^{-1}$. The parameters calibrated to this data set may be found in Table 5 in the appendix. The AAE between the calibrated model NO_x output and the measured NO_x output is 68.9387 ppm. The same parameters are applied to the estimate of NO_x output of the first data set acquired on 12/5/2011. The AAE is 59.1691 ppm. The estimated NO_x outlet using parameters calibrated to 12/6/2011 data and the measured 12/5/2011 NO_x outlet data is shown in Figure 15 below.

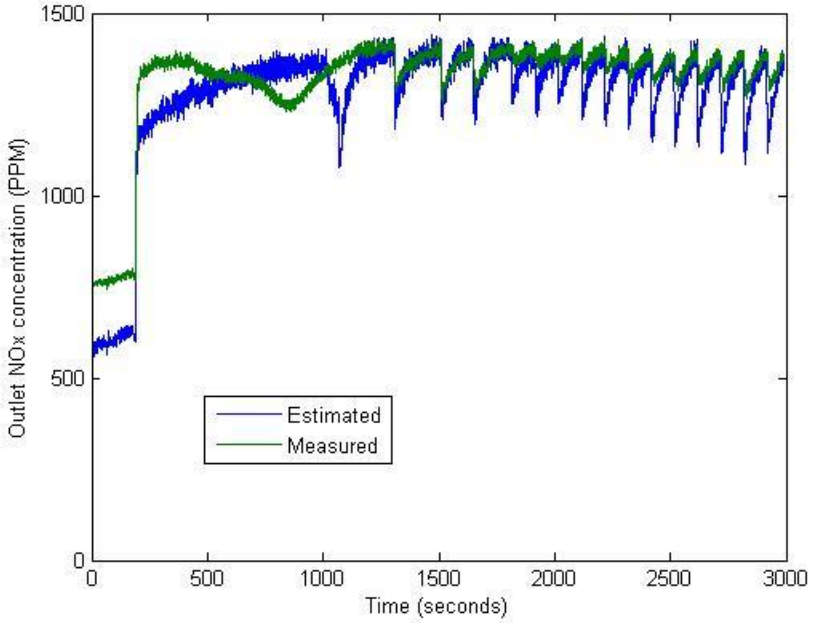

Figure 15: Estimated and measured NO_x outlet concentration calibrated using 12/6/2011 data, applied over 12/5/2011 data.

The AAE for estimating 12/5/2011 set 1 data using model parameters calibrated with 12/6/2011 set 2 data is 56.18ppm. In this specific case, the model appears to approximate the outlet NO_x concentration more accurately during injection[5], however, prior to injection the inlet NO_x conditions had not yet stabilized. This is evidenced in the sharp increase in outlet NO_x concentration at the start of the data set. Varying operating points that cause changes in inlet NO_x concentration while not injecting fuel appear as changes in the approximation of the outlet NO_x concentration. This is because the time constant within the HC-SCR model is only applied during injection events and the inlet NO_x is fed through with only an offset being applied. This demonstrates the importance of mapping the model across varying operating conditions.

The validation method is repeated for other data sets at similar flow conditions. For example, the second data set captured on 12/21/2011, includes a wide range of temperatures at a constant flow rate of $154 m^3 h^{-1}$. The outlet NO_x concentration vs. time and model parameters for this data set may be found in the appendix in Figure 28 and Table 5,

[5] Injection events can be identified as sharp periodic drops in the outlet NO_x concentration.

respectively. These parameters are applied to other data sets with similar flow conditions. This is shown in the next few figures.

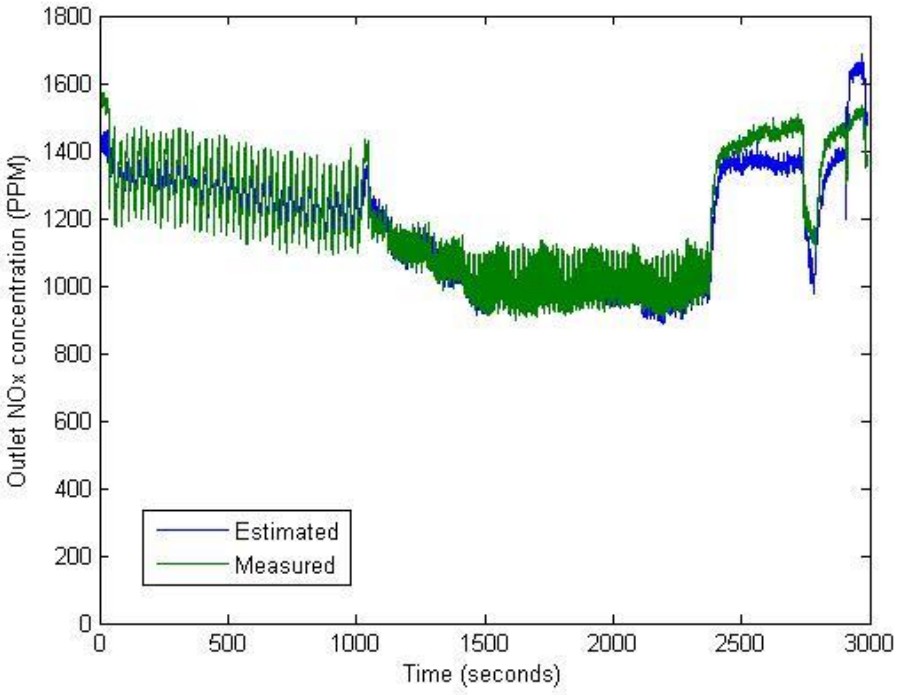

Figure 16: Estimated and measured outlet NO_x concentration calibrated using 12/21/2011 second data set, applied over 12/21/11 first data set.

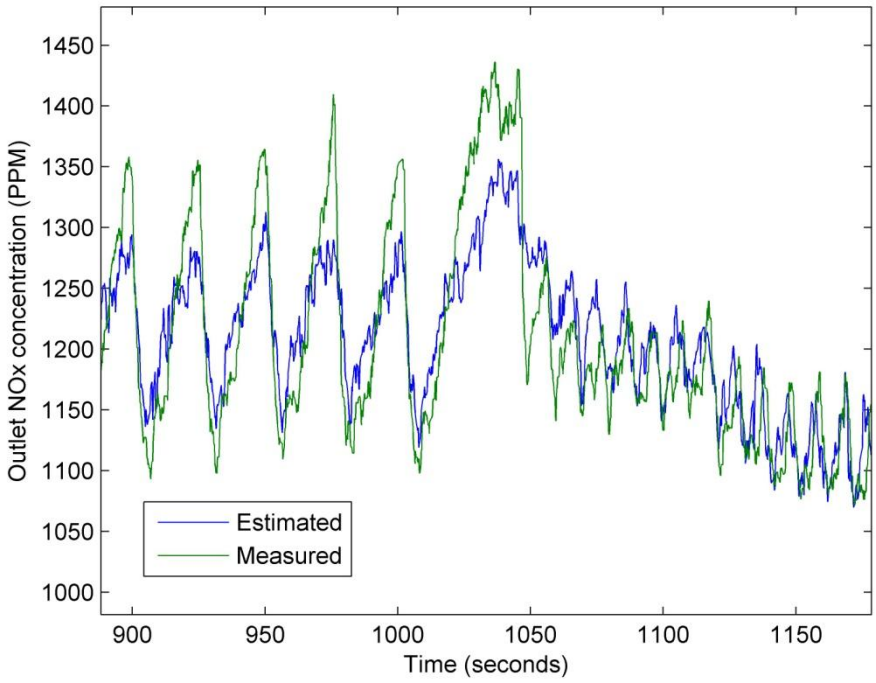

Figure 17: A closer look at a transition within estimate of 12/21/2011 first data set, calibrated using 12/21/2011 second data set.

In Figure 16 above, the AAE is 49.5334 ppm. For comparison, the AAE between the calibrated data set and the model estimation is 35.4791 ppm. A second data set is validated with the same parameters. This can be seen in Figure 18. The validating data set is the third set taken on 12/22/2011. The AAE is 29.2240 ppm.

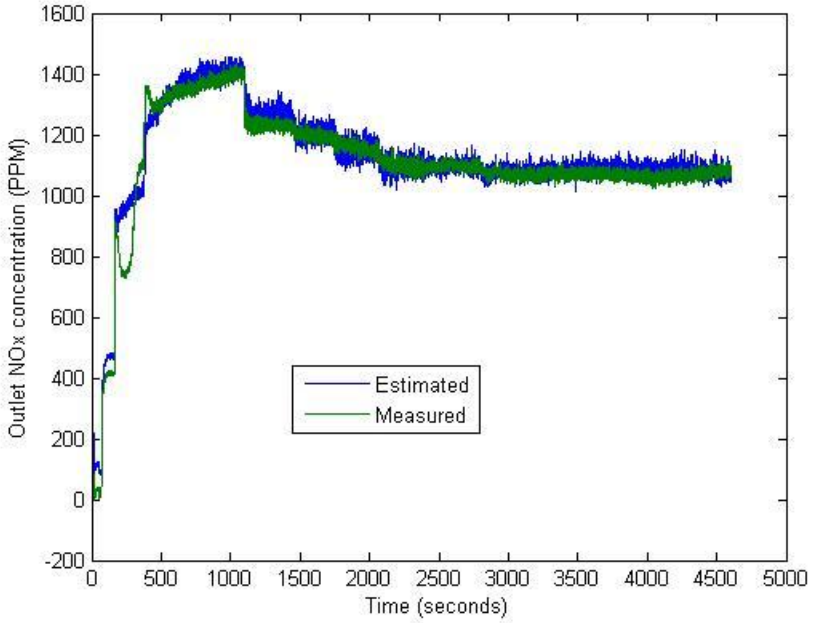

Figure 18: Estimated and measured outlet NO_x concentration calibrated using 12/21/2011 second data set, applied over 12/22/11 third data set.

The ability to apply model parameters from one data set to another and still obtain a close fit (in terms of AAE) to the data demonstrates that the model is accurate for data sets with similar flow rates.

Sensitivity analysis

When considering a model with various parameters for a system, it is important to know how each parameter impacts the system. To quantify the influence of the parameters for the current model, a sensitivity analysis is performed.

Typically, the sensitivity index of a function R is calculated as

$$\theta_i = \frac{\partial R}{\partial x_i}, \quad i = 1,2,\ldots.L, \tag{17}$$

where x represents each of the variables in the function, and L represents the number of variables [26] [27]. For this specific case, a modified version of Equation (17) is used. In this case, outlet NO_x concentration is the "R" of Equation (17), however, calculating the sensitivity index of one single point in a data set would not accurately capture the sensitivity of that parameter because of the outlet NO_x concentration's dependence on the binary

injection event signal. Because of this, AAE is chosen as the "R" in the sensitivity analysis, and the entire data set is used to obtain the changes in AAE with respect to changes in each parameter. Instead of using the continuous derivative of Equation (17), an approximation of the derivative is used in the form of a delta function. The sensitivity may be calculated as follows,

$$\theta_j = \frac{\Delta AAE}{\Delta x_j}, \quad j = 1,2, \ldots . L, \tag{18}$$

where x represents a parameter of the model, and L represents the total number of parameters in the model.

The second data set captured on 12/21/2011 is chosen for the sensitivity analysis because of its wide temperature excursions. The graphs of ΔAAE vs $\Delta parameters$ can be found in section two of the appendix. Of all the parameters, changes in ctemp and y produce the largest changes in AAE, while changes in the temperature weighting coefficients a and b produce the smallest changes in AAE. Thus the most influential model parameters can be identified as ctemp and y, while the least influential model parameters can be identified as the temperature weighting coefficients. This can be used to improve optimization speed, by prioritizing the optimization to focus on the most influential model parameters.

Health Diagnostics

The HC-SCR model may be used to identify cases where a disturbance causes the inputs to no longer correlate with the outlet NO_x concentration. This type of disturbance could be caused by a reductant failure such as a clogged supply line or an injector stuck in either an open or closed position. A reductant supply failure is shown in Figure 19.

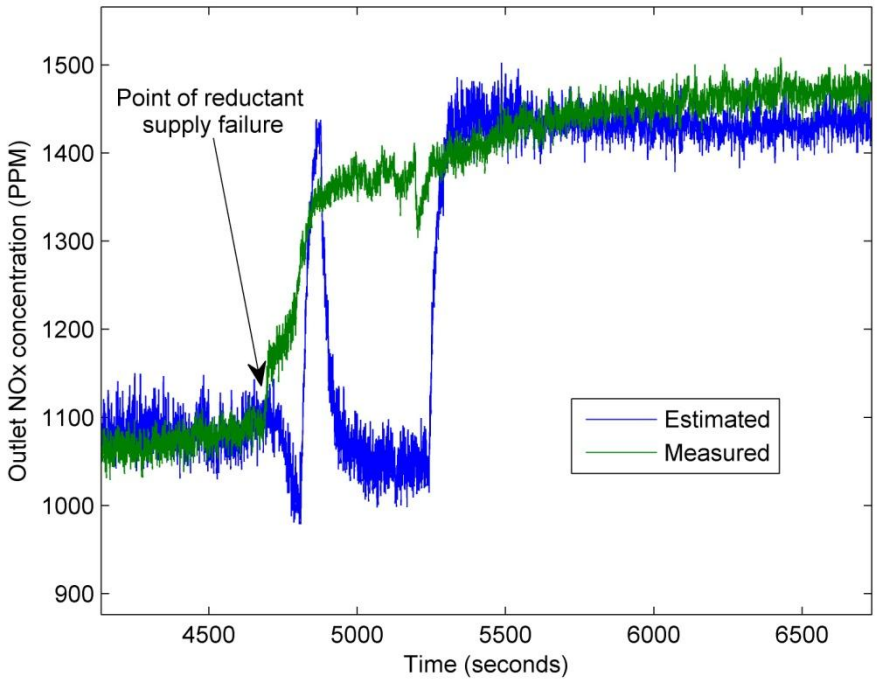

Figure 19: Estimated and measured outlet NO_x concentration during a reductant supply failure.

The reductant supply failure shown in Figure 19 illustrates how the model continues to predict the outlet NO_x concentration as if the reductant supply had not failed. It is possible to take advantage of this by adding a diagnostic NO_x concentration sensor to the outlet of the HC-SCR, and monitoring the difference between the estimated and actual NO_x.

CHAPTER V: DEVELOPMENT OF CONTROL METHODOLOGY

The SCR model developed in this work demonstrates that the reduction of NO_x across the catalyst behaves as a first order system when perturbed by a reductant injection event. Therefore, a PI controller is used for the control strategy. The controller is tuned in simulation environment using temperature and inlet NO_x data from an experiment. The injector on signal is controlled by the controller, which receives an error signal created from the difference between the desired NO_x setpoint and the feedback signal from the outlet NO_x values generated by the model. This arrangement can be seen in Figure 20.

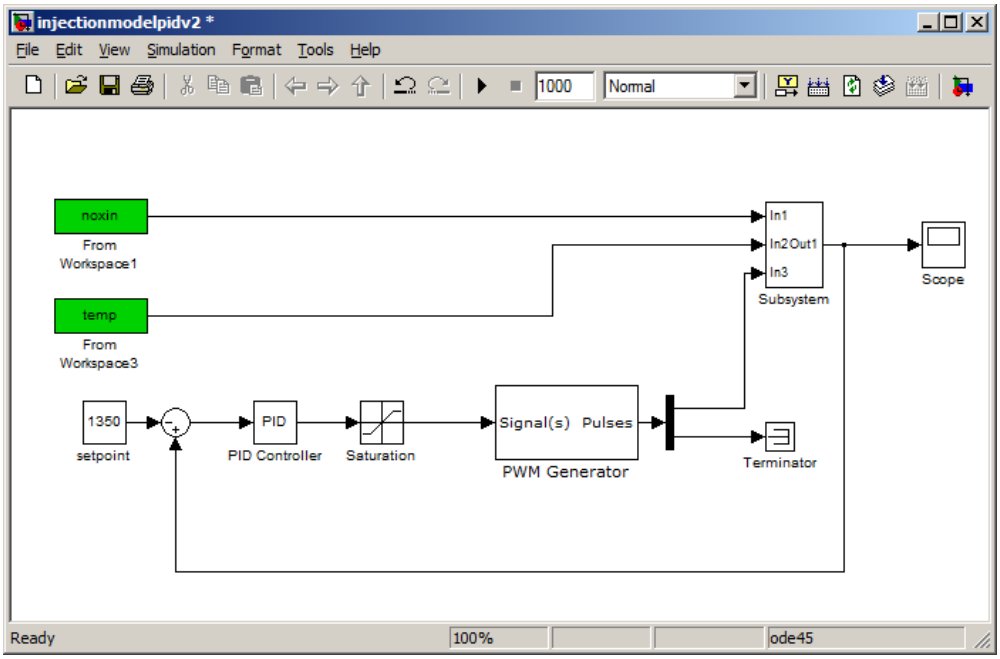

Figure 20: Simulink block diagram showing closed loop simulation of SCR.

The closed loop simulation includes a proportional-integral-derivative (PID) controller block, with the derivative gain set to zero to disable derivative behavior, effectively creating a proportional-integral (PI) action controller. A saturation non-linearity is applied to the outlet signal from the controller. This creates a signal with a value between zero and one, with a one-to-one correlation between the inlet and outlet for any value in between. The saturation block is required to condition the signal for use as a duty cycle input to the pulse-width modulation (PWM) generator. For initial analysis and tuning, the PWM block is set to produce a signal with fixed period at 25 seconds and a pulsewidth that varies with the

commanded duty cycle from the saturation block. An optimization algorithm is used for tuning the controller. This is done by setting the optimization target to minimize the error between the setpoint and the outlet NO_x value. An example of the output of the tuned controller is shown in Figure 21.

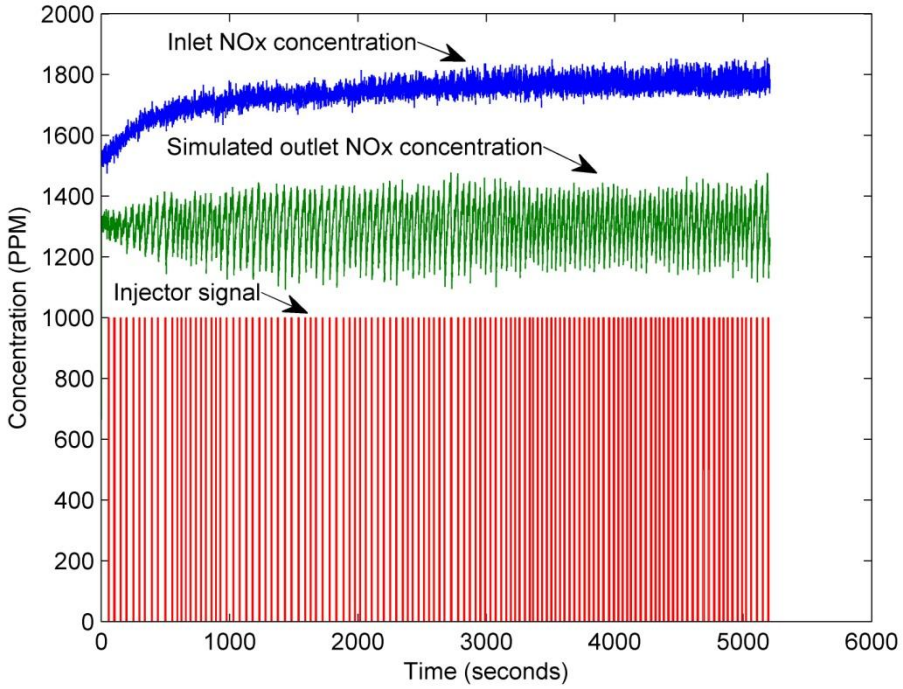

Figure 21: Simulated system under closed-loop control with 1300ppm NO_x set point.

During simulated closed loop control, a setpoint of 1300ppm results in an average injector duty cycle of 15.4%. Lowering the setpoint to values such as 500ppm with an average inlet NO_x concentration of 1800ppm causes the injector to run at 100% duty cycle until the simulated outlet NO_x reaches the setpoint. In real world conditions, this high rate of conversion is not possible. The model allows this because calibration of the model occurs within the tested regions. Testing for over-fueling would help make the model more accurate at these operating conditions.

By providing the compact Rio PLC with a NO_x outlet concentration signal, it is possible to close the loop and implement a controller on the SCR. The closed loop operation of the SCR is shown in the screen capture of the LabView environment during operation, shown in Figure 22.

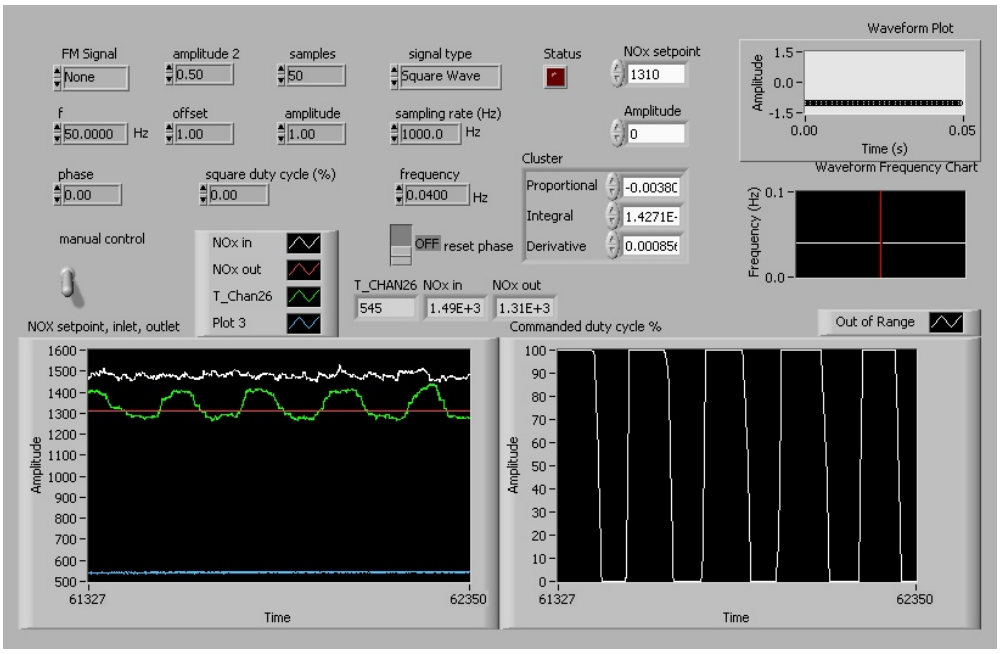

Figure 22: LabView screen capture during closed loop operation.

In Figure 22, the left-most graph displays inlet NO_x concentrations, outlet NO_x concentration, NO_x setpoint and a temperature signal. During this screen capture, the inlet NO_x concentration remains steady with some noise at roughly 1500ppm, the setpoint is constant at 1310ppm, and the outlet NO_x concentration is fluctuating about the setpoint. The graph to the right displays the control signal produced fed to the injector by the PI controller.

CHAPTER VI: CONCLUSIONS AND FUTURE WORK

Conclusions

In the previous sections a model of the outlet NO_x concentration of an HC-SCR model is developed from the known primary HC-SCR chemical reaction. This is done by assuming excess oxygen at the inlet of the catalyst and measuring the inlet NO_x, catalyst temperature, and injection event. The model is calibrated to a real world engine-catalyst combination. The model is capable of estimating the outlet NO_x concentration of the catalyst at constant exhaust flow conditions. The model incorporates a gain which directly relates to a catalyst temperature-scaled efficiency. This gain is useful in determining catalyst health, or aging. The model is validated over independent data sets and the estimated outlet NO_x is shown to correlate with the measured value to less than 70ppm AAE.

A simulation of a PI feedback controller is applied to the model and used to tune the controller gains. Implementation of the PI controller on the HC-SCR system demonstrates that it is possible to successfully target an outlet NO_x setpoint using feedback information from the outlet NO_x concentration and the upstream diesel injector to carry out the control signal.

Future Work

The HC-SCR model and control algorithm developed in this work are good starting points for more in-depth analysis. The following paragraphs will propose future work that can be done to improve the modeling and control of this system.

One key aspect of the model that could be improved upon is to account for changes in exhaust flow rate. The current model has been calibrated at various exhaust flow sites and each site produces a new set of model parameters which vary slightly. The model parameters should be mapped across these flow rates, thus producing a model that can take into account all possible conditions. A direct measurement of the exhaust flow rate would be an ideal case; however, a more realistic approach is to create an estimate of exhaust flow based on existing engine sensors.

The model in the current work is calibrated at steady state conditions. This is an area that needs improvement for implementation in transportation control systems or health diagnostics, as these vehicles operate the engines in a transient manner. Once the model parameters are mapped across flow rates, the transient results will be significantly closer since the current model would require the user to manually adjust the model parameters to account for such a change. More specifically, one approach would involve reworking the system to calculate an online adaptable injection effectiveness value (similar to the "y" gain) for recent injections to create an expected reduction value for near future injection events. This would be focused more towards health diagnostics and controls rather than characterizing the HC-SCR as a whole. This approach would also simplify the current model by eliminating the need for the temperature inputs.

Since the model is driven by experimental data, the model becomes more accurate as more operating conditions are tested. This has been evidenced by a theoretical over-fueling simulation, where more fuel is introduced into the model, and the NO_x level continues to drop. Since this was not calibrated in the laboratory, this condition is an extrapolation of conditions that were tested. Therefore, it is important to include a factor that limits the amount of NO_x reduction in the case of an injector failing in the open position.

A PI controller is used in the current work, and is cable of holding an outlet NO_x concentration setpoint with some oscillation. If the model is adapted for transient cases, the controller should be redesigned to accommodate the fluctuating conditions as well. Gain scheduling of the controller across the various flow conditions would be a minimum requirement to maintain similar performance across different conditions. A maximum injection limit should also be incorporated in the controller to prevent over-fueling the catalyst.

BIBLIOGRAPHY

[1] Heinz Heisler, *Advanced Engine Technology*. Warrendale, PA, United States of America: SAE International, 1995.

[2] Environmental Protection Agency. (2009, October) United States Environmental Protection Agency. [Online]. http://www.epa.gov/otaq/standards/light-duty/tier2stds.htm

[3] Timothy V. Johnson, "Diesel Emission Control in Review," 2008.

[4] W. Addy Majewski, *Diesel Emissions and Their Control*. Warrendale, PA, United States of America: SAE International, 2006.

[5] John B. Heywood, *Internal Combustion Engine Fundamentals*. New York: McGraw-Hill, Inc., 1988.

[6] Richard Bauder, Christian Eiglmeier, Axel Eiser, and Henning Marckwardt, "The New High-performance Diesel Engine from Audi, the 3.0l V6 TDI with Dual-stage Turbocharging," , Dusseldorf, 2011.

[7] Robert Bosch GmbH, *Automotive Handbook*, 7th ed. Plochingen, Germany: Robert Bosch GmbH, 2007.

[8] Jörn Kahrstedt, Richard Dorenkamp, Sander Kuiken, Michael Greiner, Ingo Kühne, Giampaolo Nigro, Thorsten Düsterdiek, Burkhard Veldten, and Norbert Thöm, "The new 2.0 l TDI to fulfill American emission standards in Volkswagens new Passat," in *32nd International Vienna Motor Symposium*, Vienna, 2011.

[9] Hans-Jürgen Brüne, Josef Honeder, Peter Raschl, Michael Schinnerl, and Rüdiger Tangemann, "Emission Technologies from BMW for Future Emission Legislation Worldwide," *MTZ Worldwide*, vol. 70, no. 3, 2009.

[10] Ulrich Baretzky, Wolfgang Kotauschek, Stefan Drever, Thomas Reuss, Wolfgang Ulrich, and Wolfgang Hatz, "The V10 TDI for the 24h of Le Mans," Dusseldorf, 2011.

[11] Manfred Koebel, Martin Elsener, and Giuseppe Madia, "Recent Advances in the Development of Urea-SCR for Automotive Applications," 2001.

[12] Timothy V. Johnson, "Diesel Emissions in Review," 2011.

[13] Ford Motor Company. (2012) 2012 Diesel (67l) Supplement, 3rd Printing. [Online]. http://www.motorcraftservice.com/pubs/content/~WOCF23/~MUS~LEN/33/1260l6d3e.pdf

[14] Mona Meisami-Azad, Javad Mohammadpour, Grigoriadis M. Karolos, and Michael P. Harold, "An Adaptive Control Strategy for Urea-SCR Aftertreatment System," in *American Control Conference*, Baltimore, 2010.

[15] Da Yu Wang, Sheng Yao, Mark Shost, Joon-Ho Yoo, David Cabush, David Racine, Robert Cloudt, and Frank Willems, "Ammonia Sensor for Closed-Loop SCR Control," Detroit, 2008.

[16] Michael D. Amiridis, Tiejun Zhang, and Robert J. Farrauto, "Selective catalytic reduction of nitric oxide by hydrocarbons," *Applied Catalysis B: Environmental*, vol. 10, pp. 203-

227, 1996.

[17] Richard M. Roberts Frank T. Eggertsen, "Molybdenum Disulfide of High Surface Area," *The Journal of Physical Chemistry*, vol. 63, no. 11, November 1959.

[18] Prof. Dr. S. Olivé Dr. G. Henrici-Olivé, "The Fischer-Tropsch Synthesis: Molecular Weight Distribution of Primary Products and Reaction Mechanism," vol. 15, no. 3, pp. 136-141, 1976.

[19] Michael K. Neylon, Mario J. Castagnola, Norma B. Castagnola, and Christopher L. Marshall, "Coated bifunctional catalysts for NOx SCR with C3H6 Part I: water-enhanced activity," *Catalysis Toda*, vol. 96, 2004.

[20] Craig L. DiMaggio, Galen B. Fisher, Ken M. Rahmoeller, and Mark Sellnau, "Dual SCR Aftertreatment for Lean NOx Reduction," 2009.

[21] Julie L. d'Itri and Wolfgang M.H. Sachtler, "Reduction of NO over impregnated Cu/ZSM-5 in the presence of O2," *Catalysis Letters*, no. 15, pp. 289-295, 1992.

[22] Björn Westerberg, Christian Künkel, and C.U. Ingemar Odenbrand, "Transient modelling of a HC-SCR catalyst for diesel exhaust aftertreatment," *Chemical Engineering Journal*, vol. 92, pp. 27-39, 2003.

[23] J. Rodriguez-Fernandez, A. Tsolakis, R.F. Cracknell, and R.H. Clark, "Combining GTL fuel, reformed EGR and HC-SCR aftertreatment system to reduce diesel NOx emissions. A statistical approach," *Inernational Journal of Hydrogen Energy*, no. 34, 2009.

[24] Brandon M. Dawson, Matthew A. Franchek, Karolos Grigoriadis, Robert W. McCabe, Mike Uhrich, and Smith Steve, "Automotive Three-Way Catalyst Diagnostics with Experimental Results," vol. 133, 2011.

[25] Igor Griva, Stephen G. Nash, and Ariela Sofer, *Linear and Nonlinear Optimization*, 2nd ed. Philidelphia: Society for Industrial and Applied Mathematics, 2009.

[26] Emmett P. O'Grady, "Correlation Method for Computing Sensitivity Functions on a High-Speed Iterative Analog Computer," *IEEE Trnasactions on Electronic Computers*, vol. EC-16, no. 2, 1967.

[27] Richard S. Figliola and Donald E. Beasley, *Theory and Design for Mechanical Measurements*. Hoboken: John Wiley & Sons, 2006.

[28] Ming Zheng, Graham T. Reader, and J. Gary Hawley, "Diesel engine exhaust gas recirculation—a review," *Energy Conversion and Management*, vol. 45, pp. 883-900, 2004.

[29] Sandip D. Shah, Kent C. Johnson, J. Wayne Miller, and David R. Cocker III, "Emission rates of regulated pollutants from on-road heavy-duty diesel vehicles," *Atmospheric Environment*, vol. 40, pp. 147-153, 2006.

[30] Frank Willems, Robert Cloudt, Edwin Van Den Eijnden, Marcel Van Genderen, and Ruud Verbeek, "Is Closed-Loop SCR Control Required to Meet Future Emissions Targets?," 2008.

APPENDIX

Model Parameters and Graphs

The following section contains a table showing model parameters for various data sets, figures of the each calibrated output, and sensitivity analysis graphs for each model parameter. Each set of model parameters is calibrated over sections of data occurring at constant flow rates. The figures shown in the section demonstrate the modeled and measured outlet NO_x concentration. These may be correlated with the values found in Table 5 below.

Table 5: Calibrated model parameters.

T	15.192	23.471	309.47	30.533	39.344	31.99	138.12	35.59
a	0.17209	0.095864	5.73E-07	0.00020316	2.33E-14	0.99994	2.22E-14	8.41E-07
b	1.28E-02	0.031809	1	0.0010995	2.43E-14	7.08E-06	2.22E-14	1.00E+00
c	8.27E-05	0.015417	1.73E-07	0.99334	1.00E+00	3.98E-07	1.00E+00	2.90E-02
ctemp	492.63	409.48	670.22	498.52	5.01E+02	498.52	4.99E+02	4.61E+02
d	2.427	2.434	1.62E-01	0.16219	1.60E-01	0.15601	1.60E-01	4.92E-01
offset	137.07	81.767	-59.89	-153.79	4.83E+01	-304.68	-2.53E+02	-2.16E+02
otemp	0.60666	0.24161	-7.48E-01	0.48877	4.89E-01	0.48877	4.89E-01	7.57E-01
y	-1.9251	-1.9717	-0.48705	-0.27087	-1.45E+00	-0.53874	-1.80E+00	-4.61E+00
flow m^3/h	161.8385	153.8657	3.33E+02	204.4892	170.0675	47.2927	48.6631	43.4746
aae	42.7915	35.4791	1.73E+01	30.223	19.362	27.6042	33.2756	68.9387
date	12/21/2011	12/21/2011	1/10/2012	12/19/2011	12/22/2011	12/5/2011	12/5/2011	12/6/2011
set	1	2	2	2	3	3	2	2

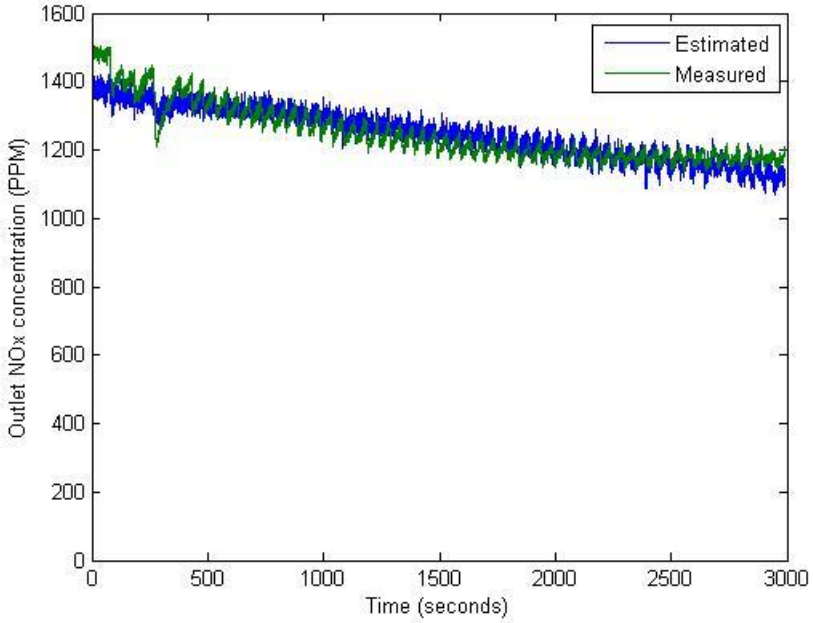

Figure 23: Estimated and measured outlet NO_x concentration, 12/5/2011, second set.

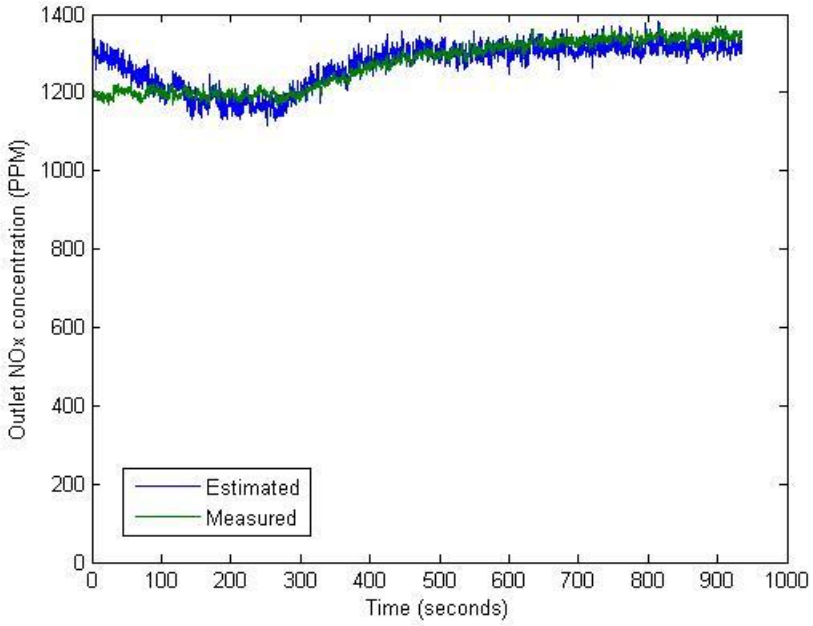

Figure 24: Estimated and measured outlet NO_x concentration, 12/5/2011, third set.

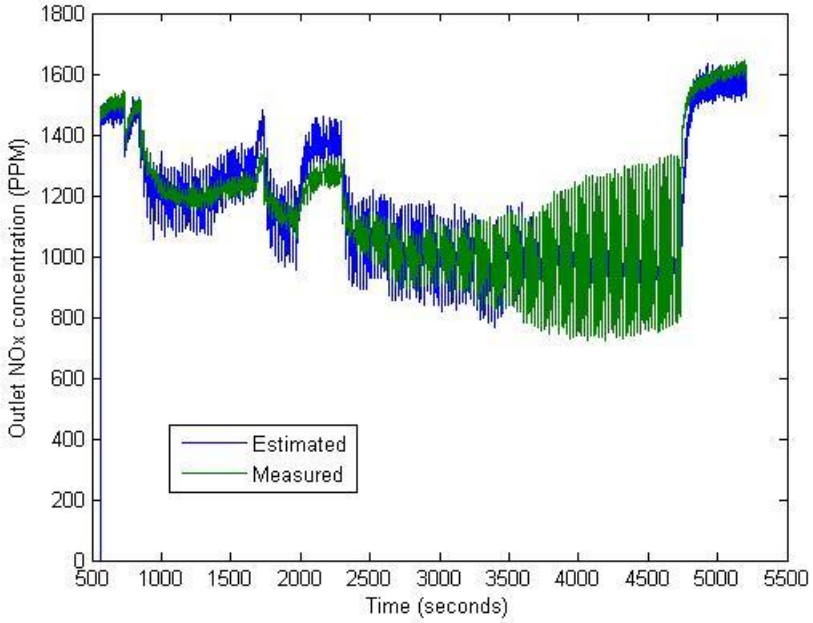

Figure 25: Estimated and measured outlet NO_x concentration, 12/6/2011, second set.

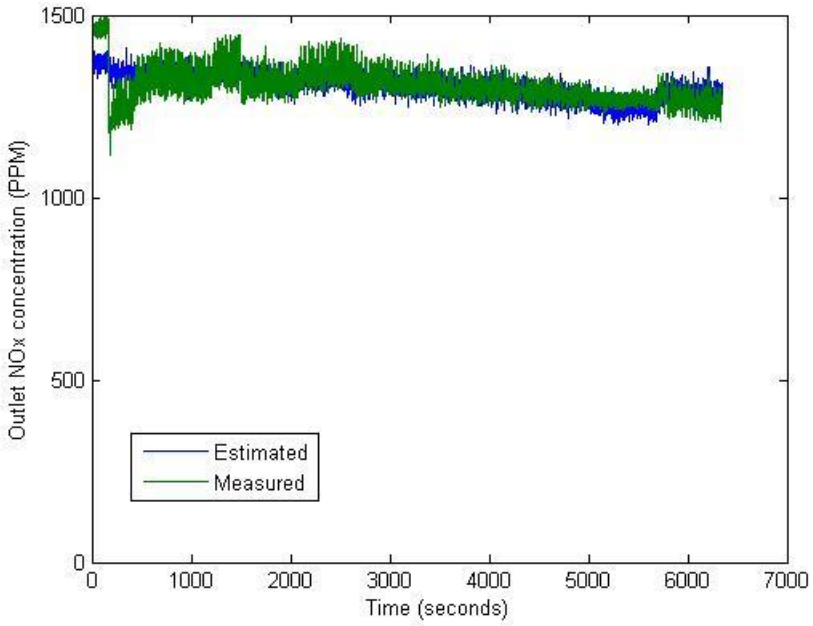

Figure 26: Estimated and measured outlet NO_x concentration, 12/19/2011, second set.

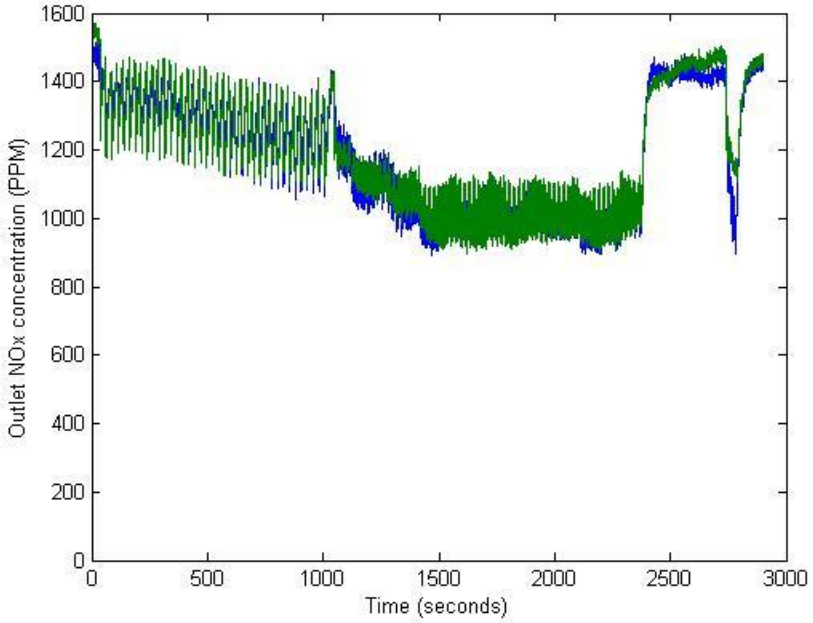

Figure 27: Estimated and measured outlet NO_x concentration, 12/21/2011, first set

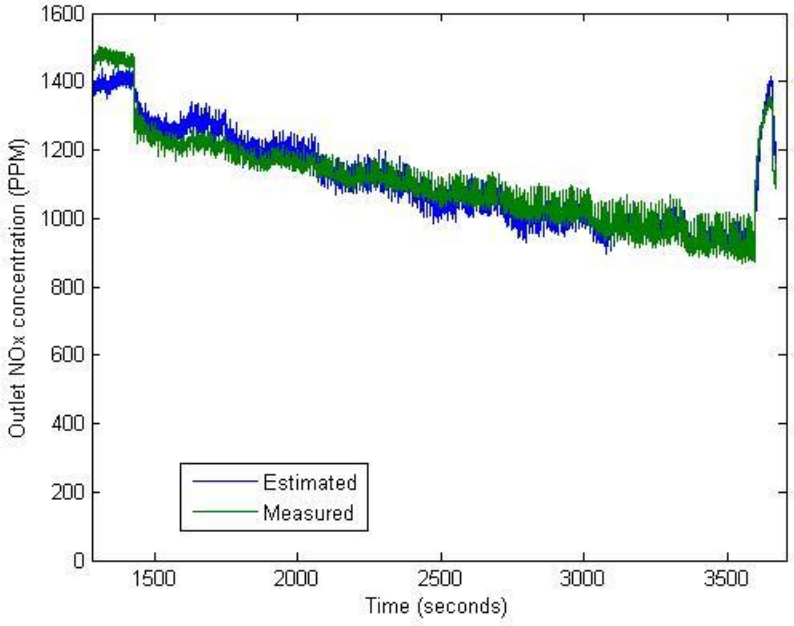

Figure 28: Estimated and measured outlet NO_x concentration, 12/21/2011, second set.

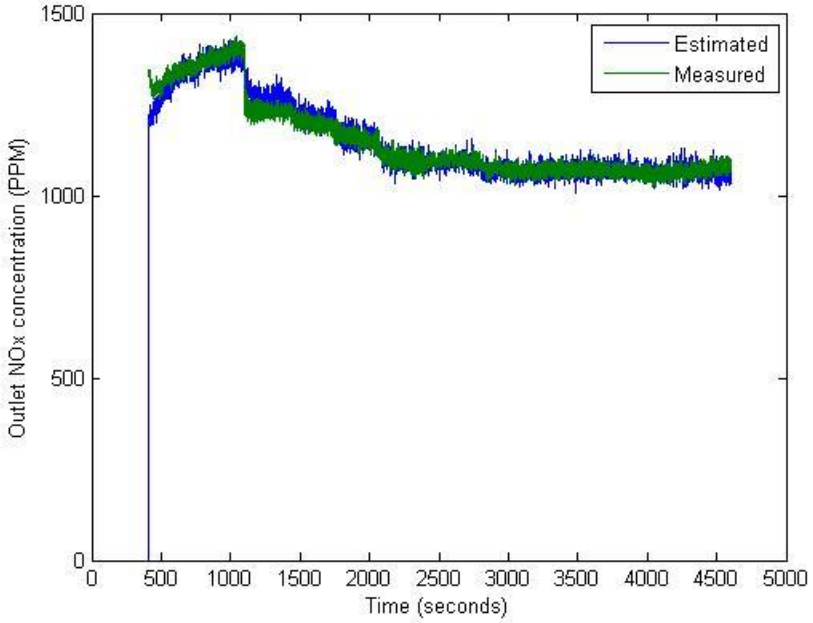

Figure 29: Estimated and measured outlet NO_x concentration, 12/22/2011, third set.

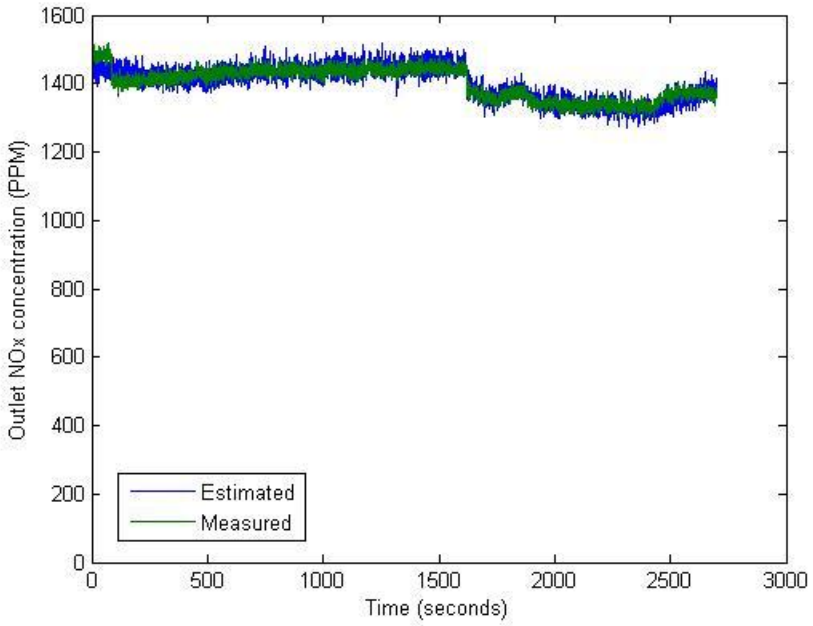

Figure 30: Estimated and measured outlet NO_x concentration, 1/10/2012, second set.

Sensitivity Analysis Graphs

The following figures were obtained by starting with the calibrated values of the second data set captured on 12/21/2011, shown in Table 5. Each figure demonstrates the effect on AAE when varying an individual parameter. Parameters are varied by 90% in each direction and the AAE is calculated at each point. The figures show the changes in AAE and parameters in their normalized forms. The percent change in AAE is calculated by subtracting the varied AAE from the non-varied AAE and dividing by the non-varied AAE and multiplying by 100,

$$Percent\ Change\ in\ AAE = \frac{AAE_{varied} - AAE_{non-varied}}{AAE_{non-varied}} \times 100. \quad (19)$$

Similarly, the percent change in parameter may be expressed as

$$Percent\ Change\ in\ parameter = \frac{Parameter_{varied} - Parameter_{non-varied}}{Parameter_{non-varied}} \times 100. \quad (20)$$

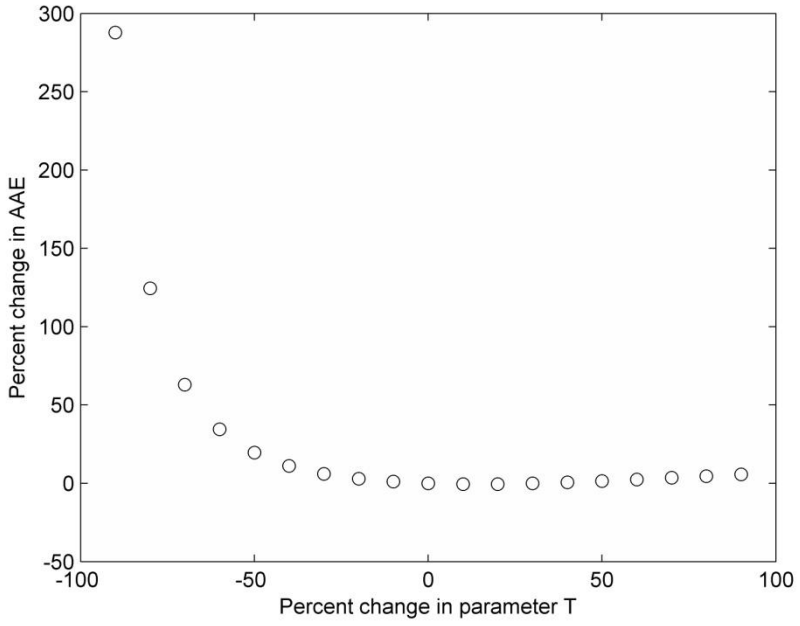

Figure 31: Sensitivity of AAE to changes in parameter T.

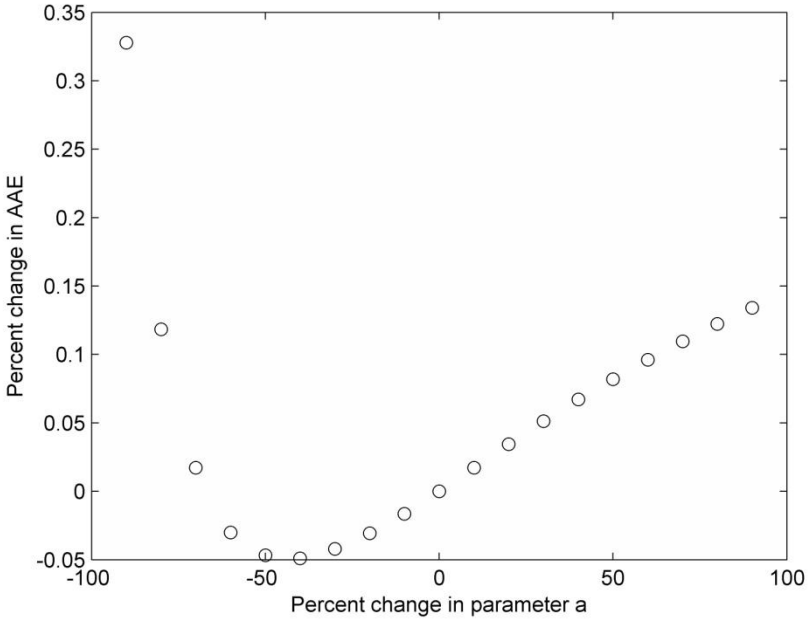

Figure 32: Sensitivity of AAE to changes in parameter a.

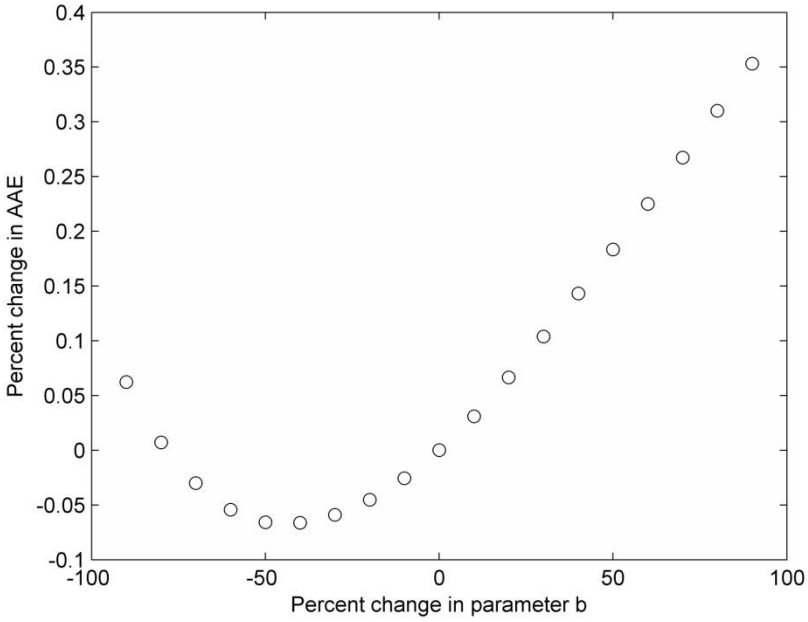

Figure 33: Sensitivity of AAE to changes in parameter b.

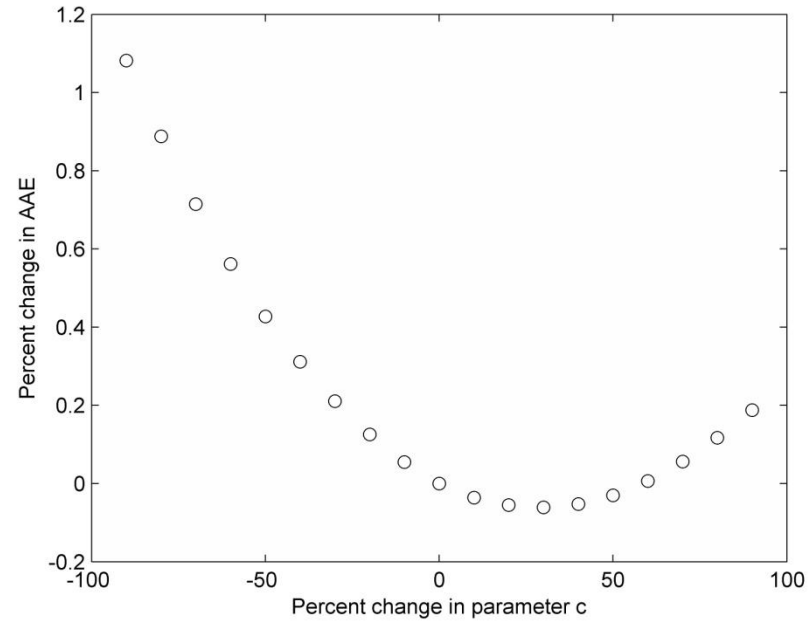

Figure 34: Sensitivity of AAE to changes in parameter c.

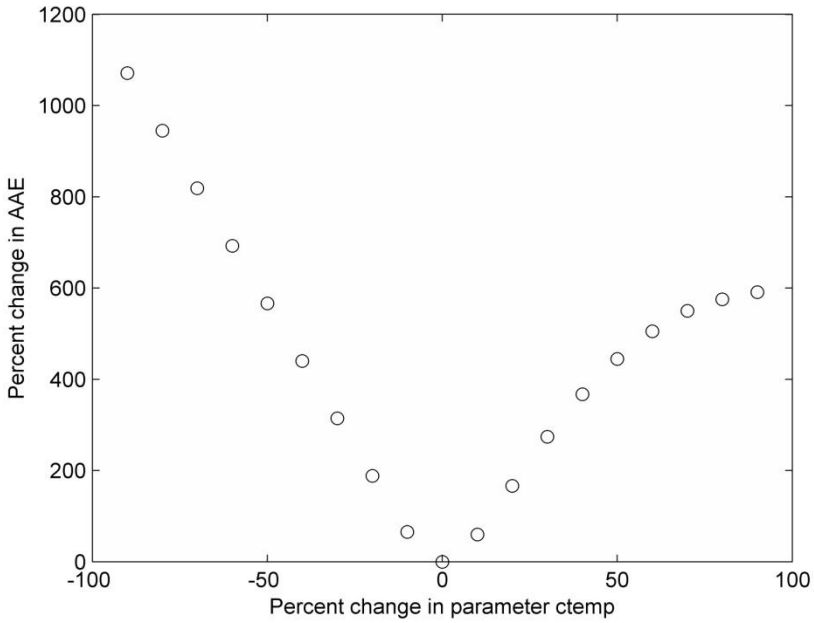

Figure 35: Sensitivity of AAE to changes in parameter ctemp.

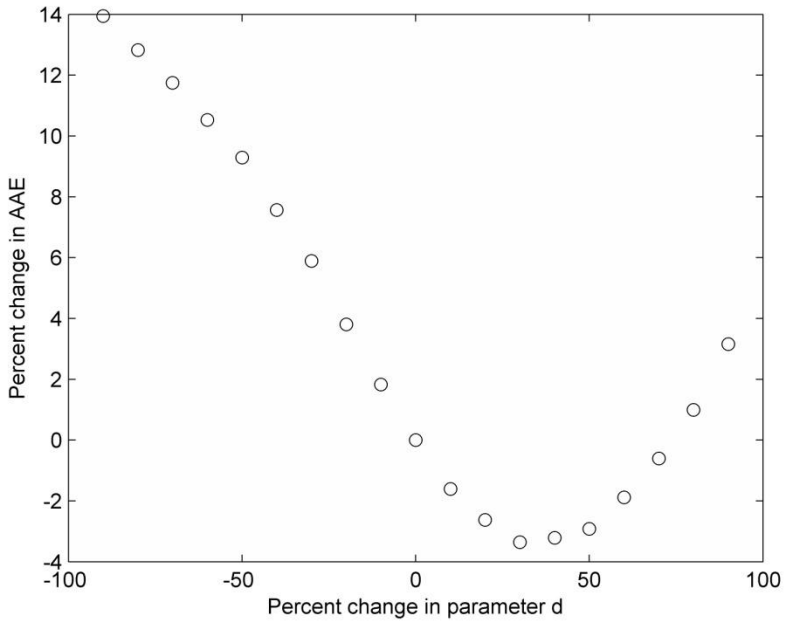

Figure 36: Sensitivity of AAE to changes in parameter d (time delay).

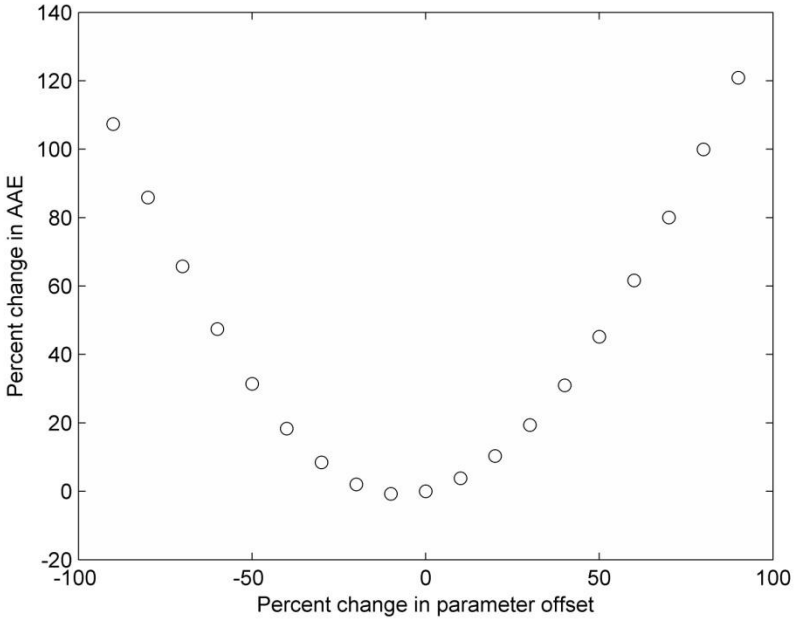

Figure 37: Sensitivity of AAE to changes in parameter offset.

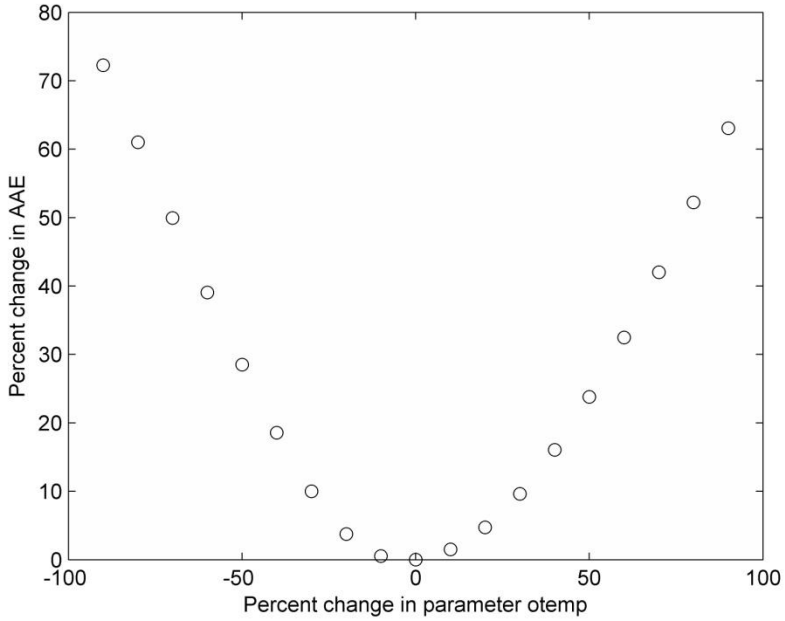

Figure 38: Sensitivity of AAE to changes in parameter otemp.

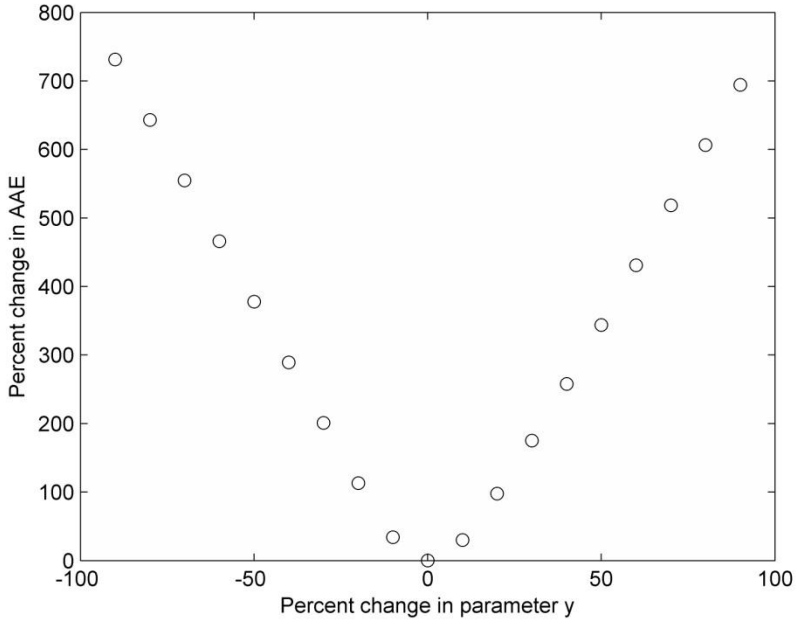

Figure 39: Sensitivity of AAE to changes in parameter y.